Evaluation of instruments for monitoring the soil-plant continuum

R. Dainese, B. de C. F. L. Lopes, T. Fourcaud, and A. Tarantino

Abstract

The response of the shallow portion of the ground (vadose zone) and of earth structures is affected by the interaction with the atmosphere. Very frequently, the ground surface is covered by vegetation and, as a result, transpiration plays a major role in ground-atmosphere interaction. The soil and the plant form a continuous hydraulic system that needs to be characterised to model the 'boundary condition' of the geotechnical water flow problem. Water flow in soil and plant takes place because of gradients in hydraulic head triggered by the water tension (negative water pressure) generated in the leaf stomata. To study the response of the soil-plant continuum, water tension needs to be measured not only in the soil but also in the plant (in addition to the water content in the soil). This paper first evaluates three instruments that can be used to measure xylem water tension, i.e. the High-Capacity Tensiometer (HCT) and the Thermocouple Psychrometer (TP) for continuous non-destructive measurement on the stem, and the Pressure Chamber (PC) for discontinuous destructive measurement on the leaves. Experimental procedures are presented and critically discussed, including data quality control and instrument calibration, accuracy, and precision. The performance of these three instruments is evaluated in terms of measurement precision and measurement accuracy via cross-validation. The paper then addresses the problem of monitoring soil

suction (pore-water tension) and water content using a second generation profile probe (fully encapsulated) and the use of Electrical Resistivity Tomography (ERT) for coarse characterisation of water content spatial distribution to support the design of spatial configuration of suction and water content sensors.

1 Introduction

The response of the shallow portion of the ground (vadose zone) and of earth structures is affected by the interaction with the atmosphere. Rainwater infiltration and evapotranspiration cause settlement and heave of shallow foundations and embankments and control the stability of man-made and natural slopes. The ground surface is very frequently covered by vegetation, which therefore represents the interface modulating the interaction between the ground and the atmosphere.

Vegetation affects directly the ground water regime in the vadose zone via transpiration. This is the process of water movement taking place from the soil through the plant up to the leaves, where water eventually evaporates through the stomata, and plays a major role in the mechanisms of water removal by the atmosphere. The soil and the plant form a continuous hydraulic system (Philip, 1966) which needs to be characterised to model the 'hydraulic boundary condition' of the water flow problem.

Understanding and modelling the mechanisms through which vegetation mediates the interaction between ground and atmosphere is key to assess climate-related geotechnical geohazards. These include rainfall-induced landslides (Gonzalez-Ollauri & Mickovski; 2017), low-rise building damage associated with drought-induced foundation subsidence (Deakin, 2005; Corti et al. 2011, Toll et al. 2012), and flood-induced instability of stream banks (Pollen et al. 2004). Vegetation can also be viewed as a 'technology' to mitigate diffuse hazard such as diffuse shallow landsliding (Alcántara-Ayala et al. 2006, Dolidon et al. 2009). Pagano et al. (2018) have shown that vegetation can lower the degree of saturation during the dry period more efficiently than the bare soil and this

reduces the pore-water pressure build-up during rainfall events thus improving the factor of safety of slopes.

The hydrological response of the soil-plant continuum is difficult to investigate in the laboratory. An experiment representative of field conditions is difficult to reproduce at the laboratory scale because of the size of plants, diversity of plant species, and the complex microstructure of the rhizosphere soil deriving from long-standing bio-chemical processes. The study of the bio-mediated interaction between the ground and the atmosphere therefore requires an open-air laboratory approach, i.e. it is the laboratory to be moved to the field and not vice versa.

This paper presents a monitoring concept for the soil-plant continuum (Figure 1) and includes instruments to monitor the water status in the plant and the ground. This system should be complemented by a weather station to monitor atmospheric variables and the reader can refer to the literature for discussion about this component of the soil-plant continuum monitoring (e.g. WMO, 2018).

The main challenges faced by geotechnical researchers and practitioners with respect to traditional geotechnical monitoring of the vadose zone are represented by the measurement of the water potential and flow rate of xylem water. The paper therefore mainly focuses on the measurement of xylem water tension by presenting and comparing the measurements by three different techniques, i.e. High-Capacity Tensiometer, Thermocouple Psychrometer, and Pressure Chamber. The paper therefore focuses on the monitoring soil matric suction using the High-Capacity Tensiometer and soil water content using a profile probe of second generation, which is fully

encapsulated and does not require the pre-installation of a casing. The paper finally discusses the use of Electrical Resistivity Tomography (ERT) to guide the design of the installation of 'local' suction and water content sensors.

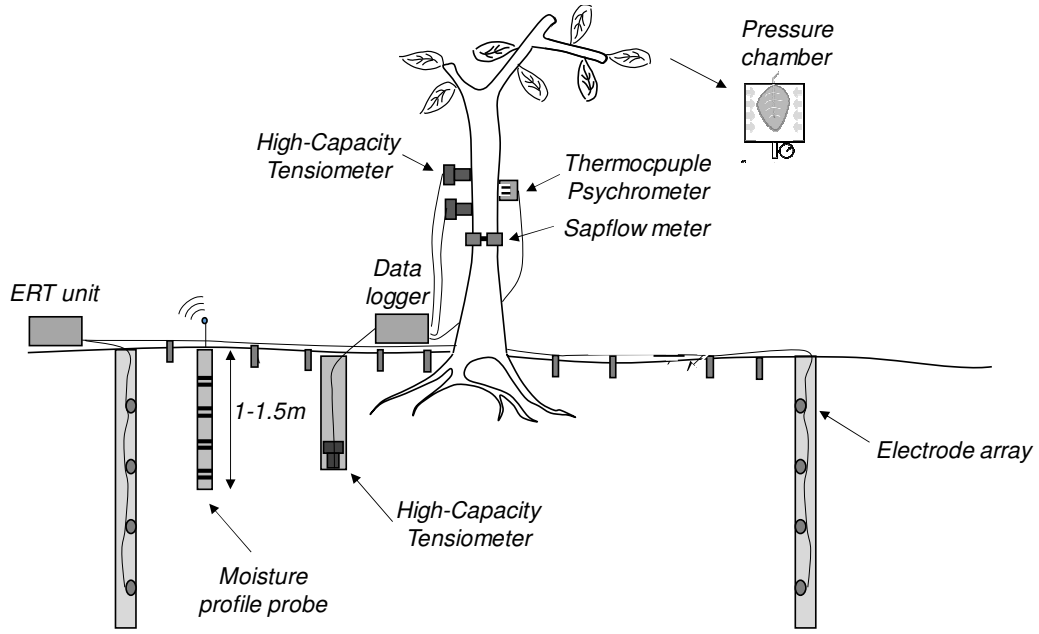

***Figure 1**. Soil-Plant monitoring system concept*

2 Measurement on plant

2.1 HCT for xylem water potential measurement

The High-Capacity Tensiometer (HCT) is composed of an integral strain gauge, a diaphragm 0.4 mm thick and a ceramic filter with nominal air-entry value of 1.5 MPa (Tarantino & Mongiovi, 2002). The working principle and the experimental procedures adopted i) to saturate the porous ceramic filter and i) to check its saturation prior to and after the measurement are discussed in Tarantino (2004) whereas details of HCT

84 installation on the stem are provided in Dainese et al (2020a). The measurement of
85 xylem water potential using the HCT has been validated by Dainese & Tarantino (2020)
86 and Dainese et al. (2020b) by comparison with Pressure Chamber and Thermocouple
87 Psychrometer on different trees and saplings. The advantage of the HCT with respect to
88 the Thermocouple Psychrometer, which is the other instrument available for continuous
89 monitoring of xylem water potential, is that its measurement is not affected by the solute
90 concentration of the sap (osmotic suction) and that the same probe can be used to
91 monitor both soil and plant. This paper discusses in detail the experimental procedures
92 to enable accurate measurement of xylem water tension.

93 An example of measurement of xylem water pressure by the HCTs is shown in Figure
94 2 for the case of a Cherry sapling (*Bigarreau burlat*). The measurement lasted 30 days
95 and two different sets of HCTs were used. HCT 5 and HCT6 were installed for the first
96 15 days (positioned 30cm and 20cm respectively above the soil) and then removed after
97 cavitation. HCT2 and HCT4 were installed on day 16 (positioned 11.5cm and 25cm
98 respectively above the soil) and were kept in place for the following 13 days. As water
99 in the xylem flows upward, the higher HCT should record in principle a lower xylem
100 water pressure than the lower HCT. This differential is not recorded for the pair HCT2
101 and HCT4, which indicates that the small difference between the two HCTs is due to
102 local variations of xylem water pressure.

103 . HCT 6 cavitated at day 11 at a water pressure of -750 kPa while HCT 5 cavitated at
104 day 15 at a water pressure of -2055 kPa. Both HCTs recorded a post-cavitation
105 measurement close to -100 kPa (-111 kPa and -118 kPa for HCT6 and HCT 5

106 respectively). Cavitation in Figure 2 appears as a vertical straight line interrupting
107 abruptly the measurement (day 11 and day 15 respectively). They then returned to a
108 value close to zero when the tensiometers were placed into free water. The detail of the
109 cavitation process is shown in Figure 3.a.

110 The very steep curves on day 1 and day 17 are associated with the hydraulic
111 equilibration between the instrument and the xylem. The saturated paste needs to lose
112 water to the xylem until equilibrium is achieved (Figure 3.b). The HCT readings during
113 the equilibration are therefore not representative of the water status of the plant.

114 The HCT measurement was considered to be valid during the first 5 days since the
115 readings of the two HCTs were overlapping. On the other hand, the measurements of
116 HCT5 and HCT6 were considered to not be valid after day 5 since the readings diverged
117 more than 50 kPa. The divergence between the two readings could be attributed to an
118 ongoing cavitation process in HCT5 or a change in xylem water pressure at the
119 measuring site of either HCT5 or HCT6. Another possible reason is the healing
120 processes occurring at the measuring site (Lev-Yadun, 2011) already observed in the
121 thermocouple psychrometer (Dixon & Downey, 2015). Since it is not possible to
122 identify, between the two tensiometers installed on the plant, the one that generated the
123 faulty measurement, the measurements of both instruments are discarded. On the other
124 hand, the measurements of the two tensiometers installed on day 16, HCT2 and HCT4
125 respectively, were always overlapping and their measurement was then considered valid.
126 The valid measurements of xylem water pressure via HCTs are reported in Figure 2 with
127 thick curves while the readings to be considered invalid are represented by thin curves.

Figure 2 shows that if only one HCT was installed on the stem between days 5 and 15, its measurement would have appeared correct because readings exhibit daily fluctuations due to the day/night cycles. The simultaneous installation of two HCTs is therefore essential to validate the measurement.

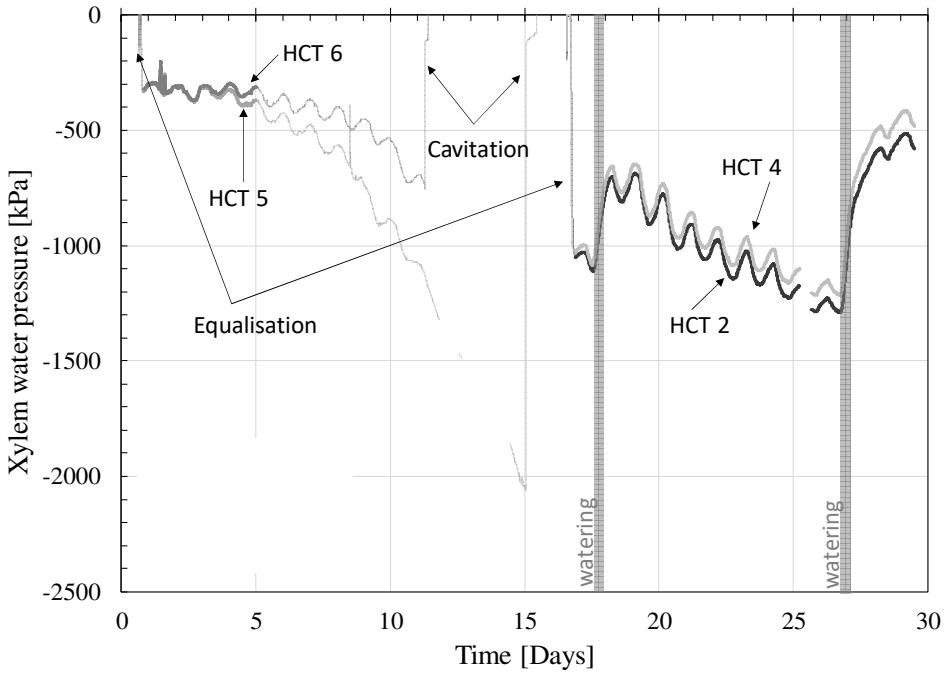

Figure 2. *Measurement of HCT on the cherry sapling. The thick lines represent the measurement in hydraulic equilibrium with the xylem, the fine lines represent the non-valid measurement of xylem water pressure.*

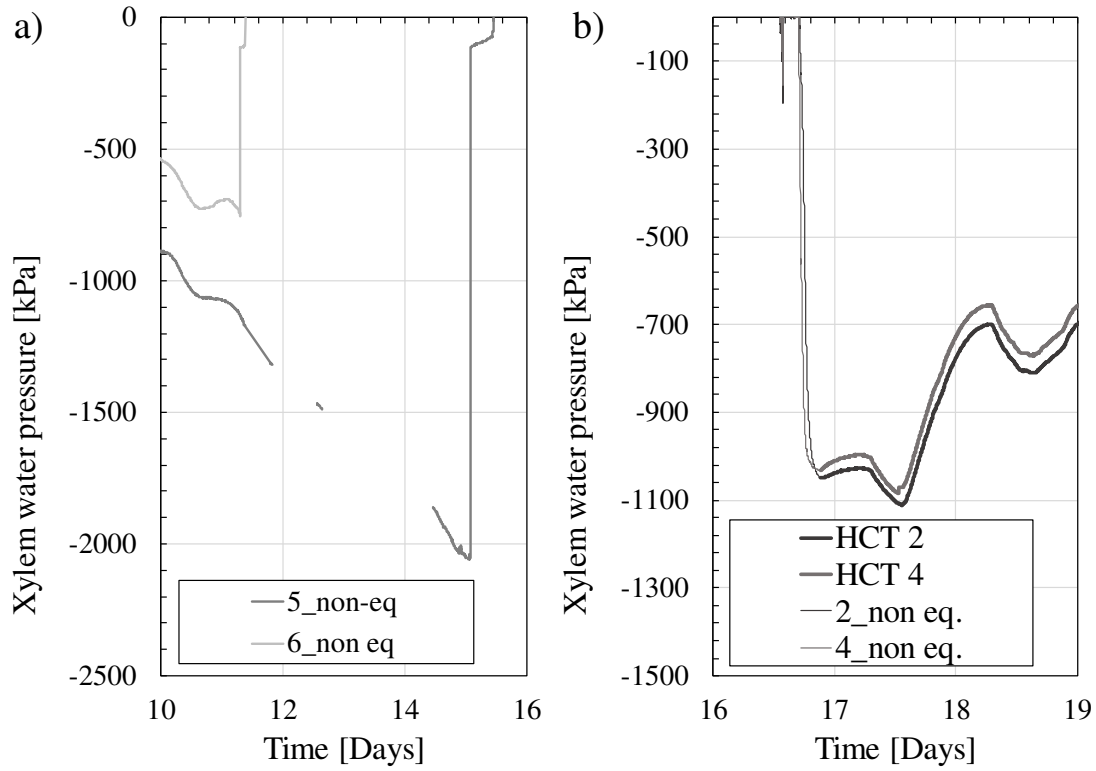

136

137 ***Figure 3.*** *Details of a) Cavitation of HCT 5 and HCT 6. b) installation and equilibration (thin*

138 *lines) of HCT 2 and HCT 4.*

139 **2.2 Thermocouple Psychrometer**

140 The Thermocouple Psychrometer (TP) considered in this work is produced by ICT

141 international (PSY1 Stem Psychrometer). The psychrometer measures the relative

142 humidity of the air in equilibrium with the xylem water, which is then converted to

143 xylem water pressure via the psychrometric law. Details of the TP working principle are

144 provided in Dixon & Downey (2015).

145 The thermocouples of the psychrometer are handmade and therefore need to be

146 calibrated individually. The manufacturer suggests to calibrate the sensor by using filter

147 paper soaked in NaCl solution. The filter paper can potentially introduce a bias due to
148 the menisci that may form at the filter paper-air interface and the matric component of
149 suction generated thereof. To investigate this potential effect three calibration systems
150 were considered: i) a bottle filled with NaCl solution with about 15 mm gap between the
151 liquid surface and the thermocouple , ii) a small cap filled with NaCl solution with
152 various air gaps (5 mm, 2 mm, and 1 mm), and iii) a filter paper soaked with NaCl
153 solution (Figure 4.a).

154 The decay of the electrical potential versus time for the 5 setups in Figure 4.a is
155 shown in Figure 4.b. The signal at equilibrium (achieved when the signal did not change
156 any longer over time) should in principle not be affected by the air gap (i.e. the distance
157 between the sensor and the evaporating surface). Nonetheless, the experimental data
158 showed the opposite possibly due to larger thermal gradients occurring in the larger
159 gaps. However, the signal tends to converge when the air gap becomes sufficiently small
160 (1mm above free solution or less than 1mm above filter paper). The results of Figure 4.b
161 was taken as an evidence that calibration using the filter paper is appropriate and the
162 thermocouple was therefore calibrated using this calibration system.

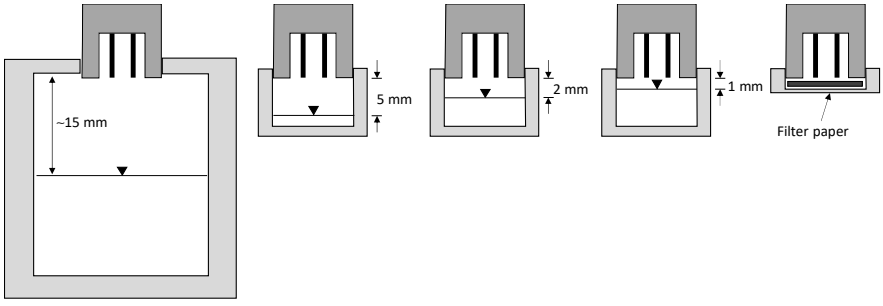

(a)

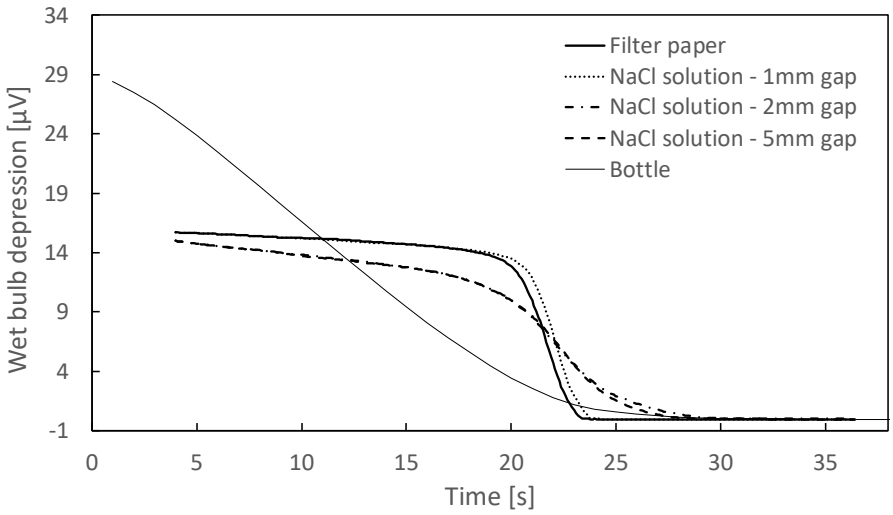

(b)

163 ***Figure 4****. Calibration of Thermocouple Psychrometer by exposure to 1.0 mol NaCl solution (-*
164 *4.55 MPa. (a) Calibration setups. (b) Effect of air gap (Cooling time = 10 sec except bottle*
165 *where cooling time was set to 20 sec)*

166 The thermocouple signal depends on the Cooling Time, i.e. the time whereby the
167 current is circulated in the thermocouple to cool the thermocouple junction and cause the
168 condensation of a water drop. The effect of the cooling time on the electrical signal is
169 shown in Figure 5. The longer the current is circulated through the thermocouple, the
170 larger is the drop condensing on the junction and the higher is the thermal inertia
171 delaying the drop in differential temperature and, hence, electrical potential.

172 It is worth noticing that the cooling time affects the signal but not the tangent at the
173 inflection point, which remains the same regardless of the cooling time. As a result,
174 calibration curves relating the water potential to the electrical response should be in
175 principle built using the slope of the tangent at the inflection point. However, the ranges
176 of start acquisition time and length of the acquisition window that can be set up using

this particular instrument do not always allow detecting the entire decay curve. It follows that another characteristic of the electrical signal should be adopted to build the calibration curve.

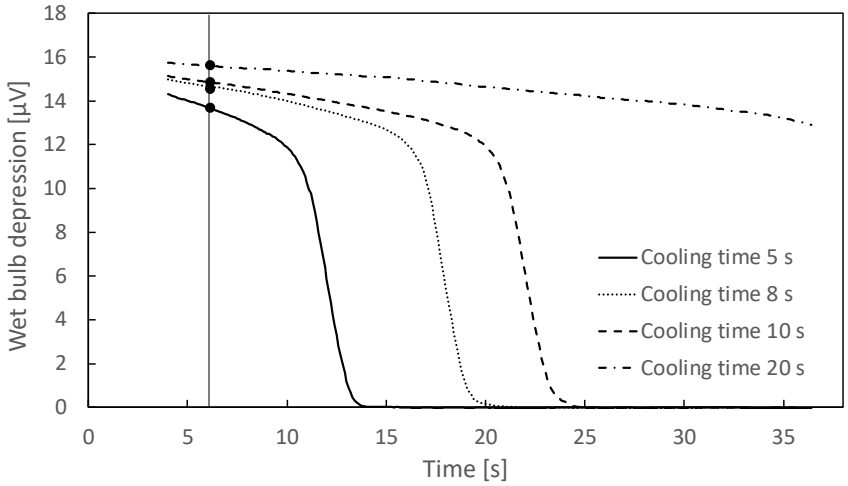

Figure 5. *Effect of cooling time (CT) on the signal recorded by the Thermocouple Psychrometer (exposed to NaCl solution of -4.55 MPa water potential (NaCl 1.0 mol)*

The manufacturer suggests to detect the electrical signal at a given time, which is referred to as Wait Time in the PSY1 manual (Dixon & Downey, 2015). However, Figure 5 shows that the electrical signal at given time (e.g. 6 s) depends on the cooling time. As a result, the decay curve returned by the instrument was investigated for two different cooling times (5s and 8s respectively). For each cooling time, two different acquisition windows were considered, 4-36 s and 13-45 s respectively, to enable a Wait Time of either 6 s (4+2 s) or 15 s (13+2 s) respectively.

Figure 6 presents the decay curves derived for two cooling times and two different acquisition windows recorded by exposing the thermocouple to NaCl solutions having

192 water potential ranging from -0.45 to -4.55 MPa (0.1 to 1 molality). The lower the water
193 potential (lower relative humidity), the lower is the temperature required to cause water
194 drop condensation and, hence, the higher is the initial voltage differential. At the same
195 time, the lower the water potential (i.e. the lower is the relative humidity), the faster is
196 the water drop evaporation and, hence the decay in voltage differential.

197 Figure 6.a and Figure 6.b show the decay curves for 8s Cooling Time and the two
198 different acquisition windows. In both cases, the signal recorded at the Wait Time
199 decreases monotonically as water potential increased from -4.55 MPa to -0.5 MPa.

200 Figure 6.c and Figure 6.d show the decay curves for 5s cooling time and the two
201 different acquisition windows. It is worth noticing that the signal at -4.55 MPa for the
202 Wait Time of 15s decays faster than the Wait Time itself. As a result, the signal recorded
203 at the Wait Time at higher lower water potentials becomes suddenly the lowest rather
204 than the highest. The correlation between voltage differential and water potential
205 therefore loses monotonicity. A relatively short Wait Time therefore need to be selected
206 to avoid a non-unique relationship between water potential and voltage differential
207 recorded at the Wait Time.

208 The calibration curve derived from an 'loading-unloading' cycle with Cooling Time
209 = 8 s and Wait Time = 6 s is shown in Figure 7. The calibration is essentially linear
210 although accuracy can be slightly improved by adopting a polynomial of the second
211 order (standard deviation of the error reduced to ±0.024 MPa from the value of ±0.046
212 MPa associated with the linear calibration).

213

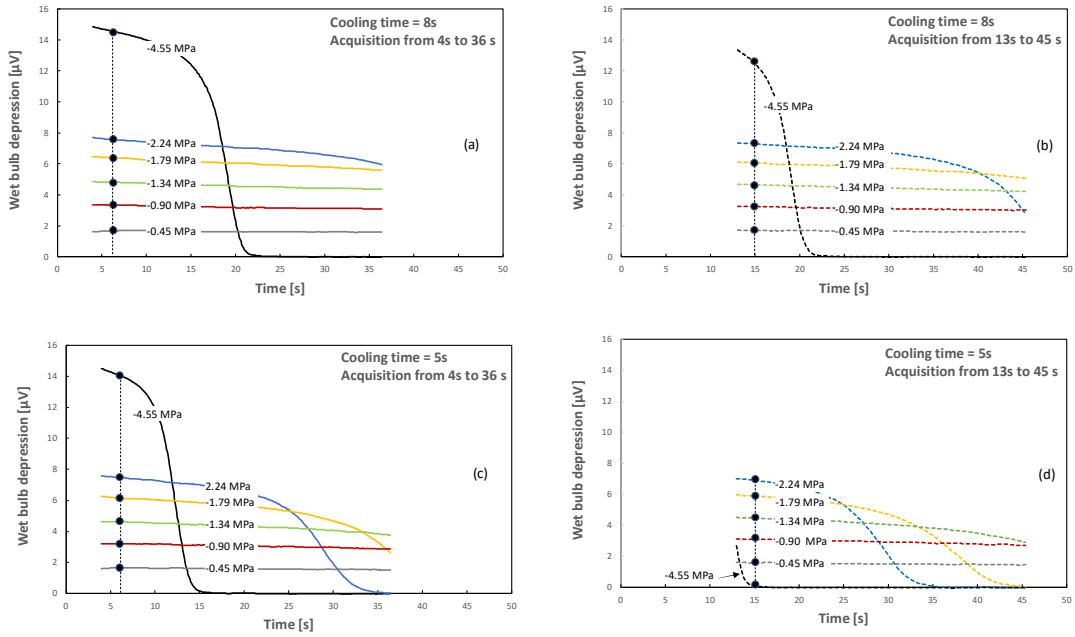

214

215 ***Figure 6***. *Effect of cooling time (CT) and Start Acquisition Time (SAT) on the signal recorded by*
216 *the Thermocouple Psychrometer exposed to NaCl solutions of different water potential. (a)*
217 *CT=8s and SAT = 4s. (b) CT=8s and SAT = 13s. (c) CT=5s and SAT = 4s. (d) CT=5s and SAT*
218 *= 13s.*

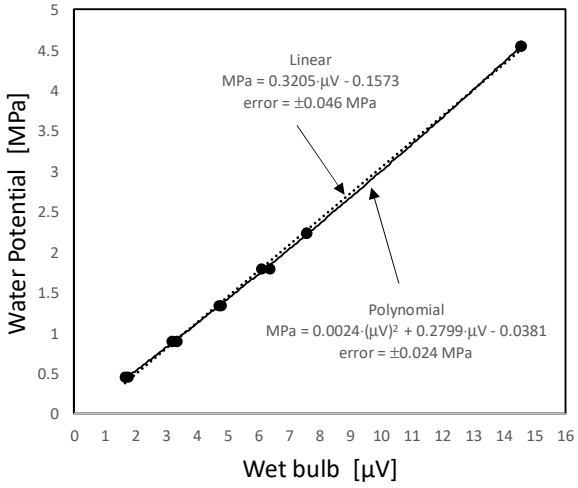

Figure 7*. Calibration curve derived from a 'loading-unloading' cycle and Cooling Time = 6s and Wait Time = 6 s*

2.3 Pressure Chamber

The working principle of the Pressure Chamber (PC) is analogous to the axis-translation technique used in soil testing (Marinho et al., 2008) and is discussed in detail in Scholander et al. (1965) and Boyer (1967). The measurement of the PC is discontinuous and destructive; the frequency of the readings is therefore conditioned by the manpower and the sampling leaves available. The PC is a commonly used and trusted technique in plant science to measure the 'xylem' matric water pressure in plants and has been often used as a benchmark to validate other techniques (Brown and Tanner, 1981; Turner et al., 1984; Balling, & Zimmermann, 1990).

The PMS 1515D Scholander Pressure Chamber (PMS Instrument, 2018) was used in this work for the xylem water pressure measurement. Leaves were initially wrapped in

aluminium foil for at least 2h. Leaf wrapping stops transpiration and allows water in the leaf to equilibrate with the branch. As a result, the water pressure recorded in the leaf is assumed to coincide with the water pressure in the branch at the base of the petiole.

The leaf was then excised with a sharp blade and promptly inserted into the pressure chamber where air was gradually pressurised until a flat meniscus formed at the end of the excised petiole (Meron et al., 1987). The air pressure in the chamber recorded when a flat meniscus appeared at the excised petiole surface is assumed to be equal to the negative water pressure in the leaf before excision.

The precision of the measurement using the Pressure Chamber is affected by the intrinsic variability between leaves and also by the subjective judgment made by the operator about the appearance of a water film at the surface of the excised petiole. To investigate the measurement precision, leaves were cut from a tree on the campus of the University of Strathclyde at three different times in a day, 8am, 1pm, and 8pm respectively (sunrise 4:45am and sunset on 9.21pm on 26 May). Two sets of six leaves were placed in the pressure chamber, the first set without removing the aluminium foil used to wrap the leaf 'in situ' before excision and the second set by removing the aluminium foil just before placing the leaf in the pressure chamber. Figure 8 shows that:

1) the precision of the measurements is satisfactory, ranging from 0.03 to 0.08 MPa in terms of standard deviation;
2) the average xylem water tension is consistently higher during the day (8am and 1pm) and lower when approaching sunset (8pm)

3) removing the aluminium foil just before the insertion in the pressure chamber leads to an overestimation of the xylem water tension possibly because of some evaporation occurring over the time the leaf remains exposed to the air.

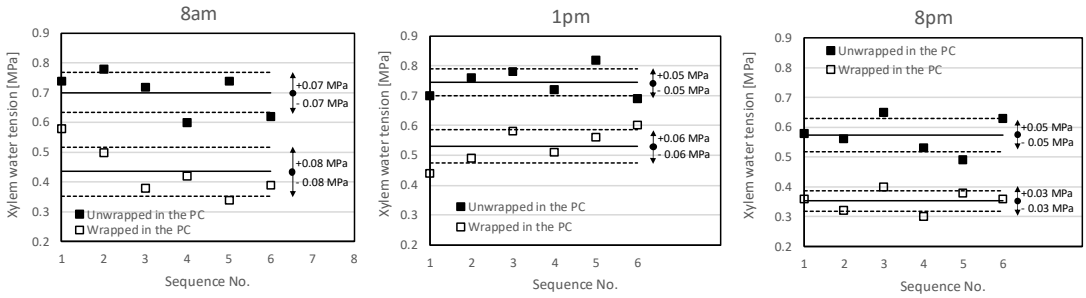

Figure 8*. Precision of Pressure Chamber measurement and effect or maintaining or removing the aluminium foil wrapping the leaf in the pressure chamber (standard deviation of the error is reported next to each set of measurements) .*

2.4 Stemflow meter

Traditional sensors used to measure the flux of sap are based on the design of the Granier's Thermal Dissipation Probe (TDP). In the original version two probes are inserted within the trunk, at a distance of 10-15 cm on the vertical axis. Each probe contains a heating element and a thermocouple. During the measurement, the higher probe (downstream to the sap flux) is heated with a constant voltage, while the lower probe (upstream) is used as a reference of the wood temperature. The difference in temperature registered by the two probes, measured in terms of difference in voltage, is influenced by the heat dissipation effect of sap flow in the vicinity of the heated probe (Lu et al. 2004). The sap flow sensor used during this study is a modification of the

TDP, where the heater and the two bead thermistors are placed within a heat-insulating hollow cylinder, and no drilling and installation of the stem is required (Anon., n.d.). The sap flow sensor used is produced by Edaphic Scientific and it is suitable for the application on small stems (1-5 mm and 4-10 mm depending on the model used).

The simplified design of the probe allows a quick installation by simply clamping the two parts of the probe around the selected twig (Figure 9). The manufacturer suggests isolating the measuring site with aluminium foil to avoid thermal disturbances. The output generated by the sensor is a voltage signal.

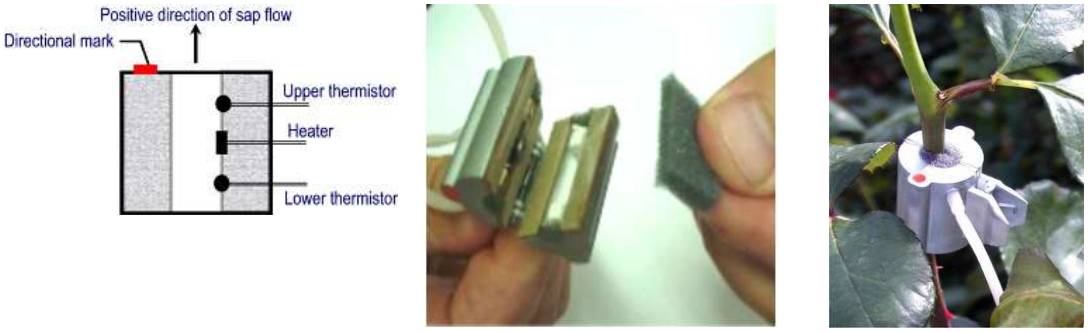

(a) (b) (c)

***Figure 9**. Stemflow meter. (a) Working principle. (b) Clamping system (c) Installation on stem.*

2.5 Comparing techniques for plant water status measurement

2.5.1 Stem-flow versus High-Capacity Tensiometer

The stemflow meter and HCT were applied on a twig and on the main stem of a 2-years old pear sapling respectively (the sapling was kept in the laboratory at constant

285 temperature). The plant was watered before the beginning of the test and irrigation was
286 stopped during the 12-day long test. The environmental conditions were kept almost
287 constant, with a temperature of 20°C±1°C and a relative humidity of 40%±5%. The
288 normal day/night cycles were mimicked by a 300 W growth lamp, providing solar
289 radiation from 6 am to 8 pm. The stemflow meter was calibrated by correlating the
290 steady-state signal recorded on selected days during day and night with the transpiration
291 rate measured by a balance.

292 Although the accuracy of stemflow meter to capture daily fluctuations of xylem
293 water flow rates could not be verified, it was deemed worth benchmarking the calibrated
294 stemflow meter against the measurement of a HCT as shown in Figure 10 (details of the
295 HCT measurement on the Pear sapling are reported in Dainese & Tarantino 2020). The
296 measurement of the transpiration rate by the stemflow was often interrupted due to
297 instability of the data acquisition system.

298 It can be observed that the sap flow meter captures the same day/night cycles as the
299 HCT. Overnight, transpiration rate attains a minimum and this corresponds consistently
300 to the highest xylem water pressure (lower xylem water tension). The transpiration rate
301 measured by the sapflow meter shows sharp increase at 6 am, when the lamp was
302 switched on and this is associated with the abrupt decrease in xylem water pressure.
303 During the day, the relationship between xylem water pressure and transpiration rate is
304 clearly reversed. Even if the stemflow meter is difficult to calibrate in the field (because
305 transpiration rate is more difficult to measure), the signal of a stemflow meter can be
306 used to assess the quality of HCT and psychrometer measurements.

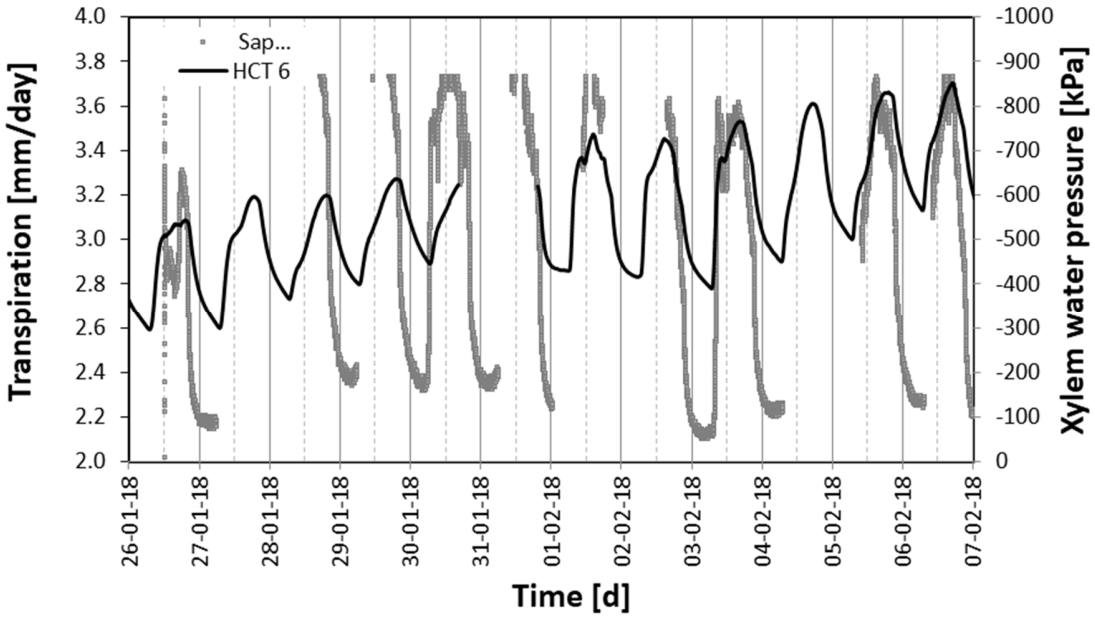

Figure 10*. Comparison of the daily fluctuation of xylem water pressure measured by the HCT on a Pear sapling against the evapotranspiration rate measure by a stemflow meter.*

2.5.2 Pressure chamber versus Chilled Mirror Psychrometer (WP4)

A comparison was made between the measurement by the pressure chamber and the WP4C Chilled-Mirror Psychrometer (Bulut & Leong 2008) by testing leaves taken from a tree on Strathclyde University campus. While on the tree, leaves were first cleaned with a tissue, wetted with a drop of distilled, gently scratched three times with sandpaper, wrapped with aluminium foil and let to rest for 10 minutes. Afterwards, leaves were excised, inserted in a plastic bag in the presence of a wet tissue to minimise evaporation (contact between the tissue and the leaves was avoided), and transported to the laboratory. In the laboratory, two sets of measurements were carried out. In the first

series, suction was first measured in the WP4C and then in the Scholander Pressure Chamber. This procedure was reverse in the second series where suction was first measured in the Scholander Pressure Chamber and then in the WP4C.

The results of this exercise are shown in Figure 11. Although a very limited number of measurements are compared, there seems to be a fair agreement between the two techniques and the sequence adopted does not seem to affect significantly the measurements and their alignment to a 1:1 line. This seems to suggest that evaporation that may occur in either the Pressure Chamber or WP4C does not affect significantly the measurement.

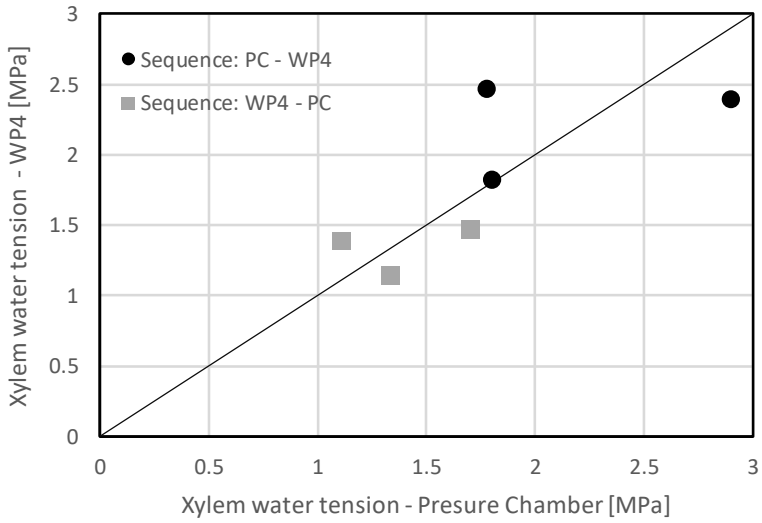

Figure 11*. Comparison of Pressure Chamber versus Chilled Mirror Psychrometer (WP4) measurements*

2.5.3 High-Capacity Tensiometer versus Pressure Chamber and Thermocouple Psychrometer

The three techniques that can be used to measure the xylem water tension, i.e. the High-Capacity Tensiometer, the Thermocouple Psychrometer, and the Pressure Chamber were benchmarked in two separate studies (Dainese & Tarantino, 2020; Dainese et al. 2020) whose results are briefly summarised here.

High-capacity tensiometer was compared to the pressure chamber via measurements of xylem water pressure on a Chestnut tree (in the field) and a Willow sapling (in the laboratory) (Dainese & Tarantino, 2020). Pressure chamber measurements on Chestnut leaves were taken on sets of six leaves, sampled from the same branch where the HCTs were installed. The leaf wrapping time was set to 10 min. Pressure chamber measurements on the Willow sapling were based on sets of three leaves with a wrapping time of at least 2h (higher wrapping time was required as the plant was under water stress conditions). The comparison between the two measurement techniques is shown in Figure 12 and the fair alignment to the line 1:1 can be taken as a cross validation of the two techniques.

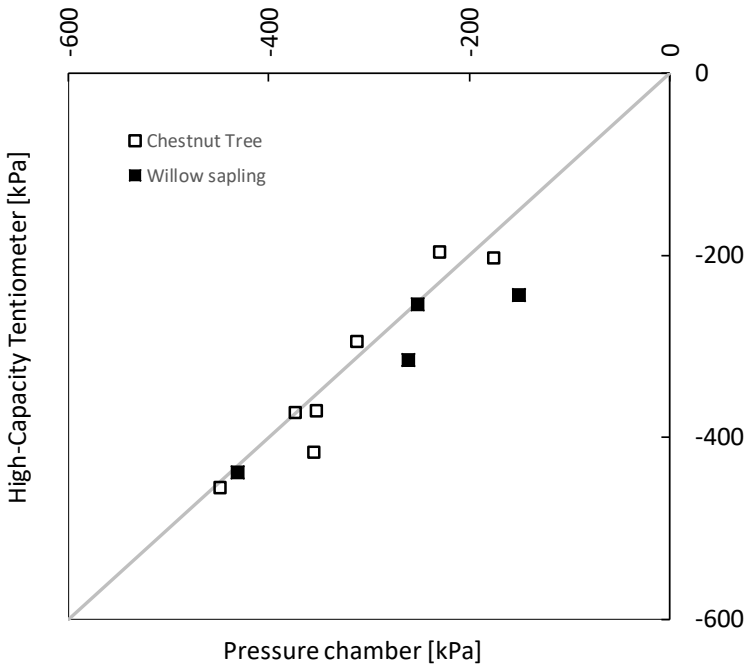

348

349 ***Figure 12***. *Comparison of Pressure Chamber versus High-Capacity Tensiometer measurements*
350 *(after Dainese & Tarantino 2020)*

351 High-capacity tensiometer was compared to the thermocouple psychrometer via
352 measurements of xylem water pressure on a Pear sapling (Dainese et al., 2020). Two
353 high-capacity tensiometers and one thermocouple psychrometer were installed with a
354 spacing of approximately 10 cm on the sapling stem with the thermocouple
355 psychrometer between the two HCTs. The measurements by the two high-capacity
356 tensiometers shown Figure 2 are replotted in Figure 13 in terms of average and only for
357 the time intervals where the measurement was considered valid. The same figure shows
358 the measurement by the thermocouple psychrometer. It can be observed that xylem
359 water pressure measurements are fairly consistent below -500 kPa and, again, this can be

taken as a cross validation of the two techniques. As discussed by Dainese et al. (2020), the thermocouple psychrometer appears to be not accurate at xylem water pressures higher than -500 kPa. In this range, the relative humidity is very close to saturation (> 99.5%) and becomes difficult to measure accurately.

Figure 13 also shows that daily fluctuations recorded by the thermocouple psychrometer and the high-capacity tensiometers are in phase. This demonstrates an prompt response time of the two instruments considering they operate on the basis of very different working principles (equilibrium via liquid and vapour phase for the high-capacity tensiometers and the thermocouple psychrometer respectively).

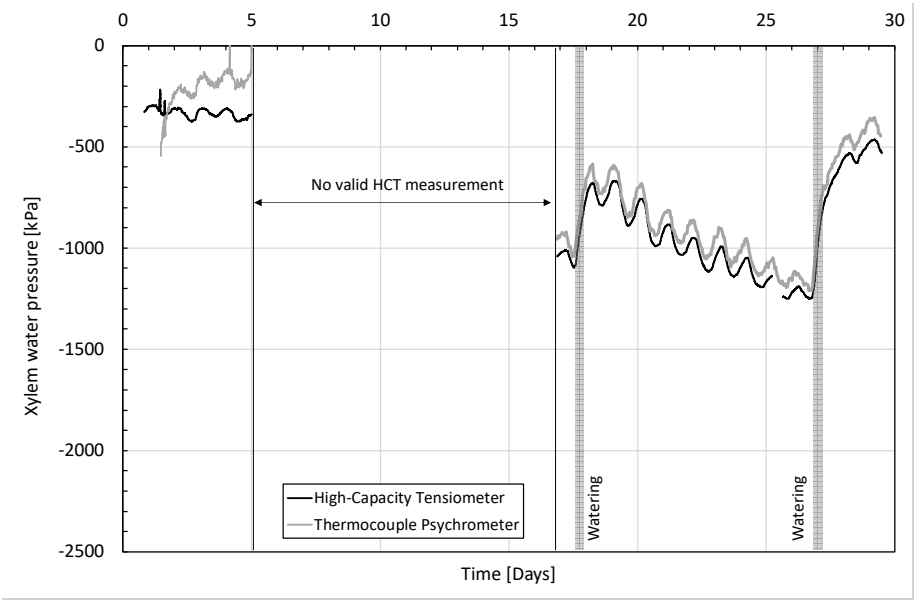

Figure 13*. Comparison of Thermocouple Psychrometer versus High-Capacity Tensiometer installed on Cheery sapling (after Dainese et al., 2020)*

3 Measurements in soil

Water flow in the vadose zone towards the plant is controlled by the soil unsaturated hydraulic conductivity (which depends on volumetric water content), and the water retention behaviour, i.e. the relationship between pore-water pressure and volumetric water content. As a result, both pore-water pressure and water content need to be monitored to characterise the water flow in the soil-plant continuum.

3.1 Pore-water pressure

Pore-water tension in the field was measured using the High-Capacity Tensiometer. Boreholes having a diameter slightly larger than the tensiometer (~20mm) were drilled in the proximity of the multi-point water content probes (described in the next section) with the aid of a manual auger. The tensiometer was mounted at the end of a rod and pushed down to the bottom of the borehole. A saturated paste made by mixing the finer fraction of the soil extracted from the borehole and kaolin was interposed between the tip of the tensiometer and the bottom of the borehole to ensure the hydraulic continuity. Evaporation from the point of measurement was prevented by the very close gap between the rod and the borehole wall. The tensiometer was left overnight to equilibrate and the measurement was taken 18-24 h after the installation.

3.2 Moisture content profile

3.2.1 Drill & Drop probe

A convenient approach to measure water content is represented by water content profile probes because a single installation can be used to capture the water content profile along a vertical. Earlier concepts (Tarantino et al., 2008) required drilling a borehole, installing a casing, and inserting the probe carrying multiple unprotected capacitive sensors into the casing. However, pouring the grout in the annular gap between the borehole and the casing often leaves air gaps that generate spurious measurements (Caruso et al. 2013). A new water content profile probe has been recently commercialised where the capacitive sensors are encapsulated into a single shaft. The performance of this probe is discussed and validated in this section. The 'Drill & Drop' probe is manufactured by Sentek Sensor Technologies, Australia, it can be up to 1.2 m long, and can include up to 12 capacitive sensors spaced 100 mm.

The working principle of the probe is based on the correlation between the bulk dielectric permittivity of the soil and its volumetric water content. The dielectric permittivity is in fact strongly influenced by the presence of water within the grains, given that the relative dielectric permittivity of pure water at 20°C is around 80, ranges between 10 and 30 for roots (Mihai et al. 2019), it is between 3 and 5 for the solid phase in most soils (Tarantino et al. 2008), and it is 1 for air. The dielectric permittivity is measured by the 'Drill and Drop' capacitive sensors through the assessment of the soil capacitance (two rings on the probe form the conductors of a capacitor filled by a composite dielectric medium that includes the soil (Dean et al., 1987).

411 The probe requires the drilling of a 25mm diameter borehole within the soil, in which
412 the probe is inserted by simple pushing. The installation procedure does not rely on the
413 use of a grout. Contact is ensured by the tapered shape of the probe, which is 25 mm
414 diameter at its bottom and 30 mm diameter at its top. This minimises the presence of air
415 gaps between the probe and the soil (compared to the grout installation of the probes of
416 first generation). The installation procedure is demonstrated by the manufacturer through
417 a series of videos (Sentek Techologies, 2019).

418 *3.2.2 Effect of roots on the measurement of dielectric permittivity*

419 Soil volumetric water content θ is inferred from the measurement of the bulk soil
420 dielectric permittivity K_a. Empirical equations are generally used to correlate K_a to θ,
421 e.g. Topp et al. (1980) and Ledieu et al. (1986). These equations have been developed
422 for the case of mixtures made of solids, air, and (free) water and may no longer be
423 applicable if a fourth phase (i.e. roots) is present.

424 The error in the volumetric water content measurement introduced by the presence of
425 roots was estimated by considering the theoretical relationship (Complex Refractive
426 Index Model, CRIM) between the soil volumetric water content θ and the bulk soil
427 dielectric permittivity K_a. This theoretical model was first validated against traditional
428 empirical equations by considering a three-phase mixture and then used to estimate the
429 error associated with the presence of roots by considering a four-phase mixture. The
430 following Equation was derived for the error in the measurement of the soil volumetric
431 water content θ (see Eq. *[12]* in the Appendix 1)

$$\Delta\theta_{error} = \frac{\sqrt{\varepsilon_a} - \sqrt{\varepsilon_r}}{\sqrt{\varepsilon_w} - \sqrt{\varepsilon_a}}\, v_r \qquad [1]$$

where v_r is the volume fraction of roots and ε_a, ε_w, and ε_r are the values of dielectric permittivity of the air, water, and roots respectively. This error is plotted in Figure 14 for the values of root dielectric permittivity that bound the range observed experimentally (ε_r=10-30).

The error clearly depends on the volume fraction of roots v_r and can be significant for high values of v_r. For the measurements presented in this paper, the volume fraction of roots in the range of depths 0-1.2 m has an average value of 0.005 with a standard deviation of 0.005 (Appendix 2). In this set of measurements, the error introduced by the presence of roots was therefore negligible.

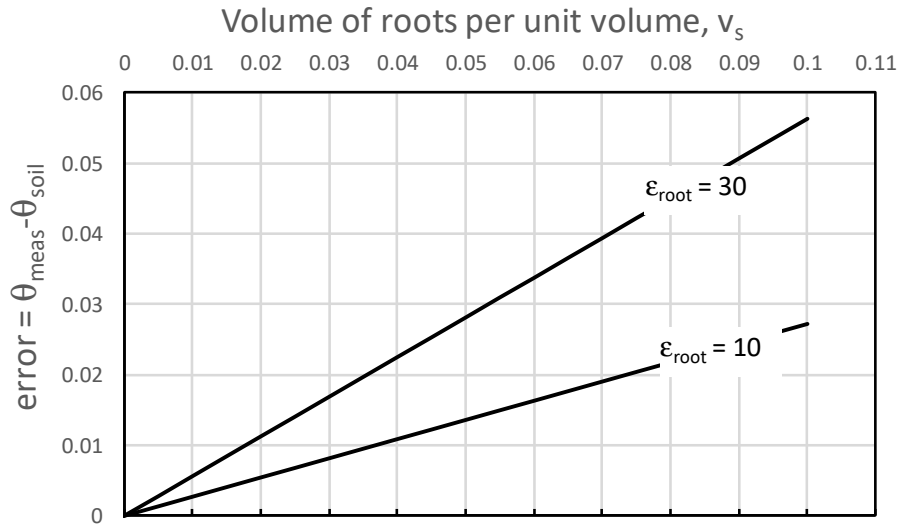

Figure 14:Error in water content measurement associated with the presence of roots

3.2.3 Effect of air gap on water content measurement

The presence of air gaps at the interface between the probe and the soil, which are minimised but not eliminated with the encapsulated probe, can severely affect the measurement, given the ratio between the dielectric permittivity of air and water is 1:80. It is therefore important to identify approaches to validate the measurement of water content.

A clear example of measurements affected or not by the presence of an air gap is shown in Figure 15, which shows the measurement by two profile probes installed in Restinclieres (France) in silty soil (20% clay, 56% silt, 22% sand), among poplar trees (Probe A) and in an adjacent open field (Probe B). The probes were installed in early July and the graph represents approximately 4.5 months of measurements.

The capacitive sensors are represented individually, ordered by the vertical position on the single probe. The number in each box represents the depth of the single sensor from the soil ground level in centimetres. There is a peak in water content of the probes in correspondence of rain events. For the case of probe A, the peaks disappear at a depth starting from 35cm (with the exception of the first rain event) whereas peaks persist down to a depth of 75 cm for probe B (encircled). While the peak in the shallow layer disappears slowly, as water drains or evaporates, spikes in the lower levels (35-75) indicate a spurious effect associated with the air gap filling with water during the rain event and quickly empting afterwards.

The effect of the an air gap on the water content measurement is represented schematically in Figure 16.a. In stage 1 and 3 the air-filled gap leads to an

underestimation of the water content measurement, while the water accumulated during the rain event leads to an overestimation of the water content of the soil surrounding the probe.

The major problem to be addressed in the water content measurement is to quantify the underestimation of measurement is stages 1 and 3 once the presence of an air gap is recognised by the peak occurring in stage 2.

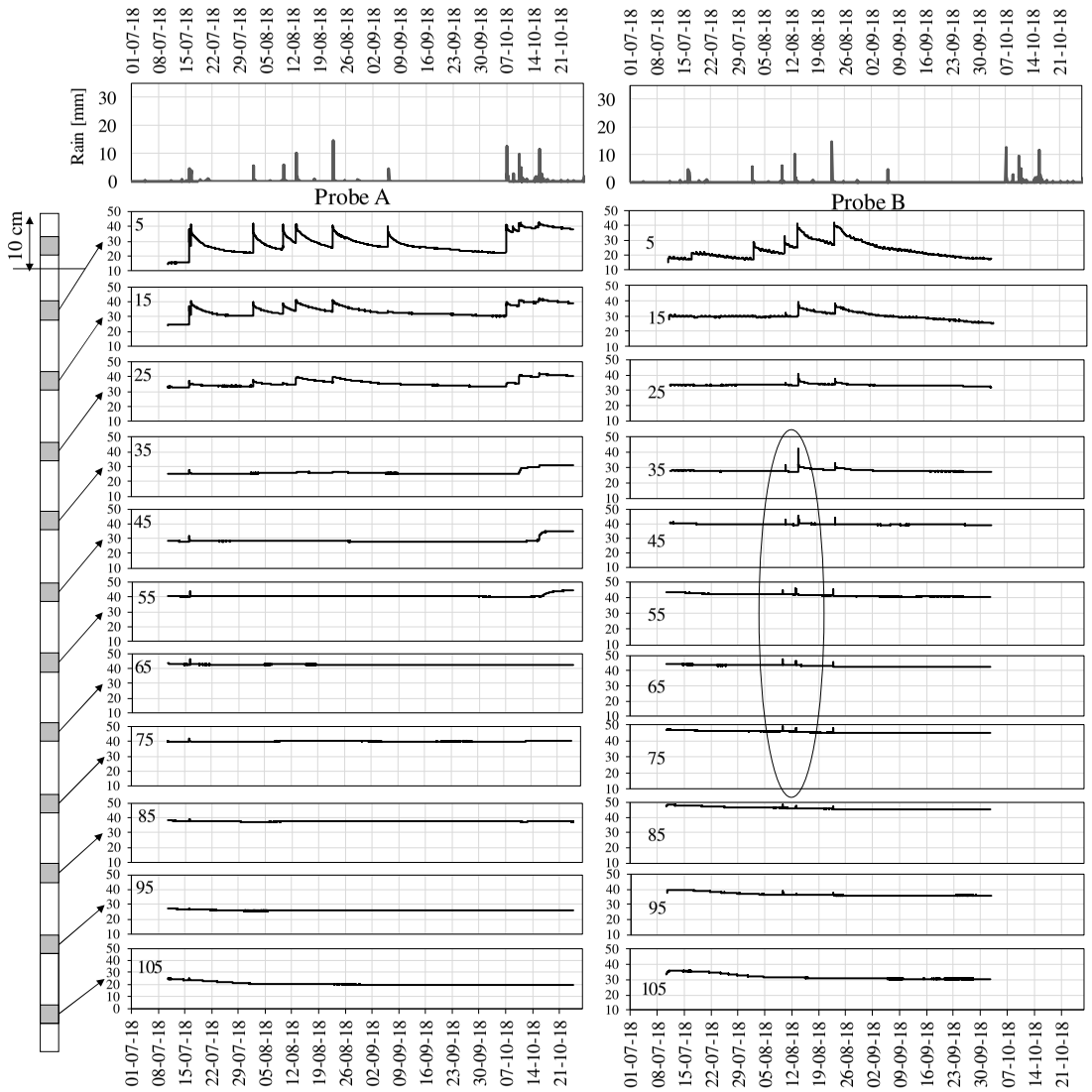

Figure 15: Representation of Volumetric Water Content evolution over time at different depths for 2 different 'Drill and Drop' probes.

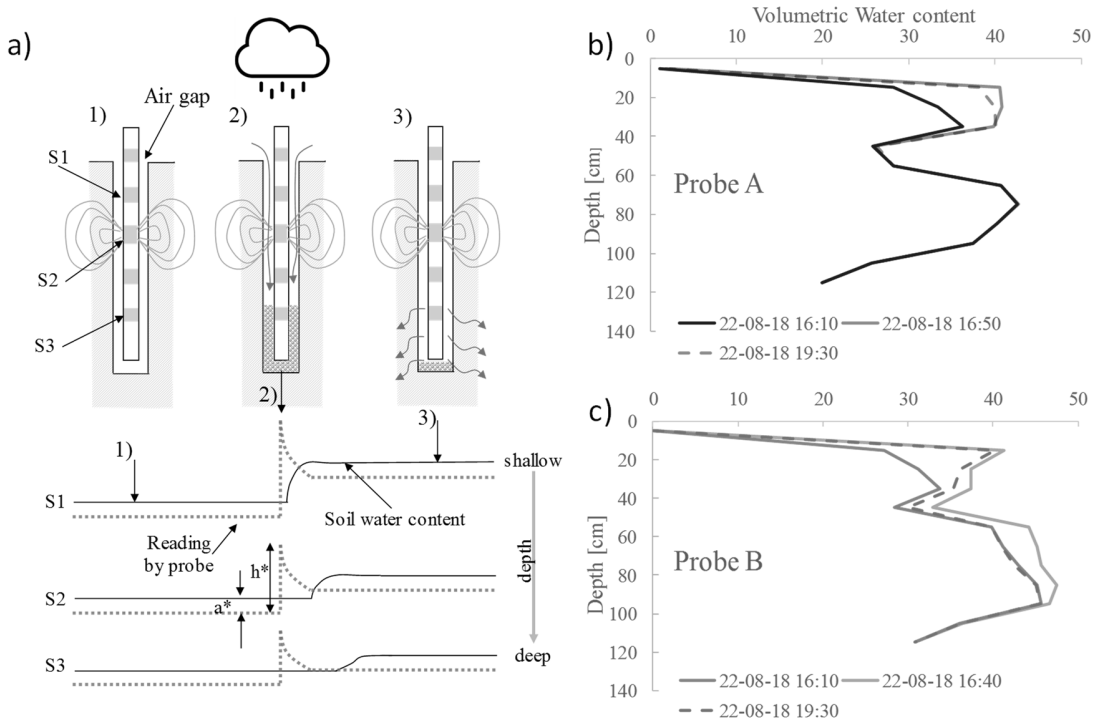

477

478 *Figure 16:(a) Effect of air gap on measurement (a.1) before, (a.2) just after, and (a.3)long after*
479 *a rain event. Water content profile in correspondence of stage a.1, a.2 and a.3 during the rain*
480 *event of the 22/08/18 for (b) probe A and (c) probe B*

481 *3.2.4 Assessing experimentally the error associated with the presence of air gap (from*
482 *water balance)*

483 The experimental data were analysed with reference to the rain event occurring on the
484 22/08/2018 for probe A (Figure 16.b) and probe B (Figure 16.c) respectively. The rain
485 event was registered by a CIRAD weather station placed at approximately 1 km distance
486 was characterised by an amount of 14.7 mm (volume per unit area) and occurred
487 between 16:00 and 17:00 (the time resolution of the weather station is 60 min).

488 The three water content profiles correspond to the condition before the rain (time
489 16:10), after the rain event showing the maximum water content variation (times 16:40
490 or 17:10), and ~3h after the rain event (time 19:30). The amount of infiltrated rainwater
491 can be in principle derived from the integration of the change of water content profile
492 measured before and after the rainfall. The rainfall amount estimated by the probe is
493 compared with the actual rainfall amount in Table 1.

494 For the case of probe A, the measurement of infiltrated rainwater after
495 approximately 3 hours (stage 3 minus stage 1) is comparable with the measurement at
496 the peak (stage 2 minus stage 1) indicating a negligible air gap. This is confirmed by the
497 close match between the actual rainfall amount and the one inferred from the profile
498 probe.

499 For the case of Probe B, the amount of rainfall derived from the water content
500 profile at peak (36.2 mm, stage 2) is significantly higher than the one derived after ~3h
501 (13.9 mm, stage 3). This indicates again that the water content profile measured by
502 Probe B at peak (stage 2) is biased by the presence of water accumulating in the gap
503 between the probe and the surrounding soil (water content accumulated in the ground at
504 peak and after ~3h should not be significantly different). The water accumulation
505 inferred from these measurements is consistent with the anomalous peaks recorded by
506 the relatively deep sensors as shown in Figure 15.

507 Although it appears evident that the measurement at peak should be discarded, the
508 problem to be addressed is whether the presence of an air gap is affecting significantly
509 the measurements in stages 1 and 3. This question can be easily answered by comparing

510 the infiltrated rainwater derived from Probe B after ~3 h with the actual rainfall amount,
511 13.9 mm versus 14.7 mm respectively. The straightforward conclusion is that the
512 presence of the air gap does not affect significantly the measurement of the water
513 content profile once water is no longer filling the gap.

514

515 *Table 1: Rain event on 22/08/2018. Comparison of volume of rainwater per unit area calculated*
516 *from 'Drill & Drop' measurements with rainfall amount.*

	Based on Raw data		Corrected for air gap	
	At peak [mm]	After ~3 h [mm]	At peak [mm]	After ~3 h [mm]
Probe A	17.4	15.6	15.6	15.7
Probe B	19.2	13.9	13.5	14.2
Rainfall amount (by weather station)			14.7 mm	

517 *3.2.5 Estimating the error associated with the presence of air gap from using*
518 *dielectric permittivity mixing model*

519 An approach to assess the effect of the air gap on the water content measurement is
520 presented here that does not require the comparison with the actual rainfall amount,
521 which may not be always available. The volumetric water content returned by the probe,
522 $\theta_{measured}$, is based on the measured apparent dielectric permittivity $K_{measured}$. According to
523 (Ledieu et al. 1986), the following correlation can be established:

$$\theta_{measured} = a \cdot \sqrt{K_{measured}} - b \quad [2]$$

where a and b are empirical coefficients (a=0.1138 and b=0.1758). The dielectric permittivity read by the probe is generated by the dielectric permittivity values of the soil and the gap (filled with either water or air) weighted by their volume fractions. As a first approximation, the following mixing model can be considered:

$$\sqrt{K_{measured}} = \frac{x_{gap}}{L}\sqrt{K_{gap}} + \frac{L - x_{gap}}{L}\sqrt{K_{soil}} \quad [3]$$

where x_{gap} is the gap between the probe and the surrounding, L is the radius of the cylindrical sampling volume around the probe (L=10 mm), K_{soil} and K_{gap} are the dielectric permittivity values of the soil and the gap respectively. For each of the three stages considered, the soil dielectric permittivity can be written as:

$$K_{soil,i} = \left(\frac{\theta_{measured,i} + b}{a} - \frac{x_{gap}}{L}\sqrt{K_{gap,i}}\right) \cdot \frac{L}{L - x_{gap}} \quad [4]$$

with i=1 to 3 and $K_{gap,1} = K_{gap,3} = K_{air}$, and $K_{gap,2} = K_{water}$. In turn, the volumetric water content of the soil θ_{soil} can be associated with the soil dielectric permittivity:

$$\theta_{soil} = a \cdot \sqrt{K_{soil}} - b \quad [5]$$

Let us assume that the water accumulating in the gap in stage 2 infiltrates radially into the sampling volume of radius L. The volume balance equation can therefore be written as follows:

$$\pi\left[L^2-\left(r_p+x_{gap}\right)^2\right]\left(\int\theta_{soil,3}\,dz-\int\theta_{soil,2}\,dz\right)-h_{probe} \qquad [6]$$

$$\cdot\,\pi\left[\left(r_p+x_{gap}\right)^2-r_p^2\right]=0$$

where r_p is the radius of the probe. The four Equations [4] and [6] can be used to derive the four unknowns $K_{soil,i}$ and x_{gap}. The left-hand side of Equation [6] is plotted versus x_{gap} in Figure 17. The gap resulting from this calculation is 0.7 mm for Probe A and 2.2 mm for Probe B. This gap can be then used to correct the values of water content measured by the probe via Equations [4] and [5]. As shown in Table 1, the values of rainfall amount derived in stages 2 and 3 are now comparable and very close to the actual rainfall amount.

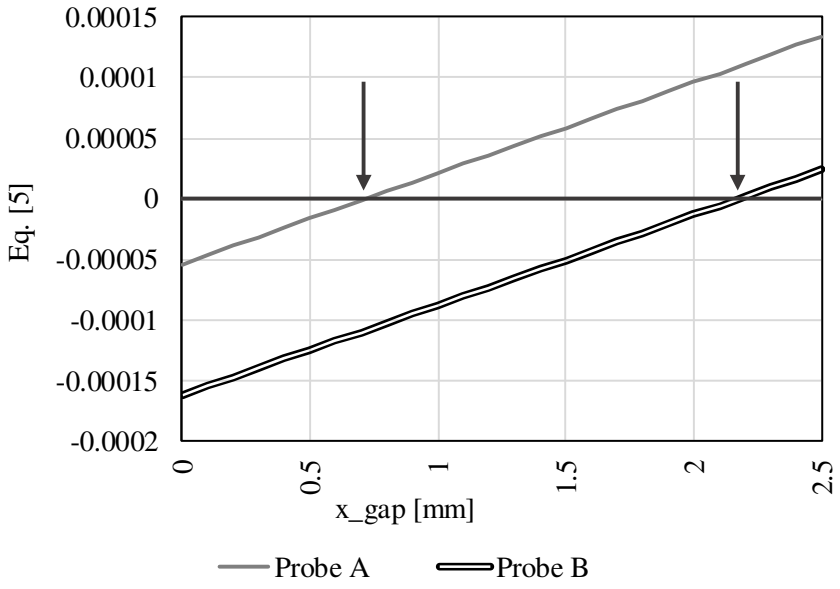

Figure 17:Estimation of the air gap

3.3 Field versus laboratory water retention data

Figure 18 shows the water retention data of Restinclieres soil measured in the laboratory on samples taken from the field via boreholes drilled close to the probes and in the field. Suction measurement in the laboratory was conducted using a chilled mirror psychrometer (WP4C). The void ratio and the gravimetric water content (used to derive the volumetric water content) were derived by pushing a cutting ring into the sample, trimming the excess material, determining the total volume from the inner size of the cutting ring, and oven-drying the sample. Some of the samples were was dried and some wetted to explore a wider range of suction. Suction in the soil at various depths was measured via the High-Capacity Tensiometers, as previously described, while the volumetric water content was assessed via the Probe A placed in proximity of the suction sensors. Volumetric water content data were paired with suction measurement data taken at similar depth.

Figure 18 shows a fair agreement between laboratory and field data. Water retention data are quite scattered due to the intrinsic heterogeneity of a natural deposit conditions.

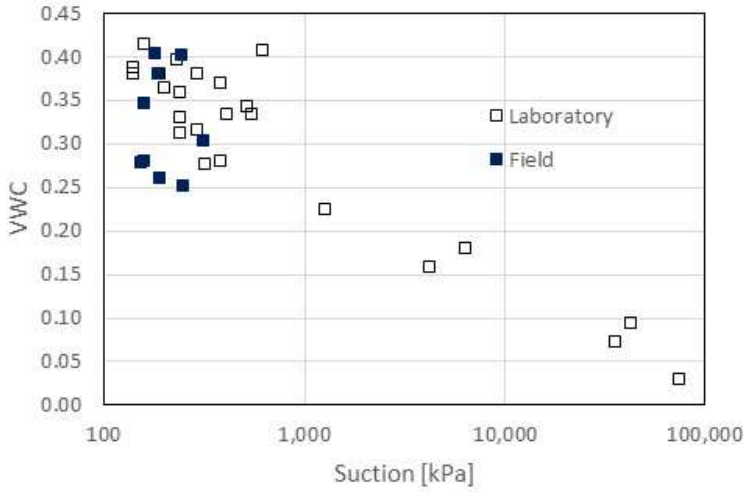

562

563 *Figure 18:Comparison of water retention data measured in the laboratory and in the field*

564 # 4 Electrical Resistivity Tomography to guide installation of local
565 sensors

566 ## 4.1 Concept idea

567 Local sensors such as such as the 'Drill and Drop' and the HCT and other local sensors
568 for measurement of suction and water content (Tarantino et al. 2008) offer the
569 possibility of investigating the variation of moisture content and suction in the field.
570 However, there are two major challenges concerning the design of monitoring systems
571 based on local sensors: (i) where to install the sensors to ensure that the local
572 measurement is representative of the area to investigate and (ii) how to extrapolate the
573 spatial distribution of measured localised variables. These issues can be addressed
574 successfully by integrating the geotechnical monitoring with electrical geophysical

575 survey (Electrical Resistivity Tomography - ERT). Electrical resistivity is a function of
576 multiple parameters including water content, mineralogy, pore structure, chemical
577 composition of pore fluid, and temperature (Samouëlian et al., 2005). However, the
578 tendency of decreasing resistivity with increasing water saturation makes this method
579 appealing for measuring a variety of different hydrologic processes. Conventional ERT
580 surveys have been used in many applications to monitor changes in moisture content
581 patterns, including around trees (Fan et al., 2015; Cassiani et al., 2015, 2016; Consoli et
582 al., 2017; Mary et al., 2018). Thus, preliminary ERT surveys can be of great help to
583 characterise an area or a geo-structure and optimise location of moisture sensors.

584 **4.2 Investigating resolution by inverting synthetic model**

585 The imaging of electrical resistivity in the subsurface by ERT is based on the inversion
586 of a set of resistance measurements on a given array of electrodes. Given the
587 nonlinearity of the underlying forward problem, electrical inversion schemes proceed in
588 iterations through modelling runs looping forward, comparing predicted and measured
589 data, and updating the estimate of the electrical resistivity distribution with a view to
590 reducing data misfit. In this work, all forward and inversion modelling was performed
591 using ResIPy v2.2.2 (Blanchy *et al.,* 2020).

592 To examine whether the ERT could help address these two key challenges, synthetic
593 models for the forward modelling exercise were created based on the observations made
594 by Dainese (2020) at an experimental agroforestry plot used for agricultural studies in
595 Restinclières, France. The author monitored the distribution of moisture content over

596 wet and dry periods by installing ‘Drill and Drop’ sensors in different locations in the
597 forestry plot and in the open field. Three different water regimes were observed close to
598 the trees, in the depth ranges of 0-50cm, 50-100 cm, and >100cm. In the first 50cm
599 depth, moisture increased (from 0.2 to 0.35 volumetric moisture content) in the wet
600 period, and decreased (from 0.35 to 0.25) in the dry period. Between 50 and 100cm there
601 was no changes in moisture content. In the wet period, below 100cm, a decrease of
602 moisture (from 0.25 to 0.2) was observed extending below the 120cm depth of the ‘Drill
603 and Drop’ and that could not be obviously detected by the sensor. Additionally, the
604 author also noticed changes in moisture on the first half meter depth, laterally away from
605 the tree (increasing in the wet period and decreasing in the dry) and below 1m depth
606 (decreasing in both wet and dry periods).

607 It was realised ‘a posteriori’ that the probe should have been installed deeper and
608 the question was asked about whether a preliminary ERT investigation would have
609 helped identifying in advance the zones where moisture content changed significantly.
610 In other words, whether the ERT could resolve the soil moisture regime down to 1m,
611 which is the length of the Drill and Drop’ sensor.

612 The approach pursued in this paper was to generate synthetic ERT data
613 representative of the observations made by Dainese (2020) and compare the inverted
614 ERT model with the original synthetic one. Synthetic models are those in which
615 resistivity values are assigned to elements of the mesh created according to the problem
616 it is representing. This model is then forward modelled (via ResIPy), i.e. the apparent
617 resistivity pseudosection is calculated for the defined 2D subsurface model. Finally, the

618 data generated by the forward model are inverted producing the inverted model, which
619 can then be compared with the original synthetic model created.

620 The resistivity values chosen to represent the water content differences observed by
621 Dainese (2020) were based on a Time Domain Reflectometry (TDR) survey carried out
622 at Rest and Be Thankful site in Scotland (Gladin, 2018). In this survey, TDR probes
623 were installed on the scar of a vegetated hillslope. TDR data was acquired after probes
624 installation and after an artificial rainfall simulated by pouring water from the top of the
625 slope. Results demonstrated that for the clayey silt material at the site, a volumetric
626 water content of 0.2, 0.3 and 0.4 correspond to a resistivity of 400, 215 and 150Ωm
627 respectively. If the middle resistivity value (215Ωm) is established as the reference, then
628 the remaining values are representative of 0.1 increase and decrease of moisture content.

629 Thus, these synthetic models (Figure 19.a-c) have a background of 215Ωm and a
630 few regions of lower or higher resistivity depending on the period it represents. Figure
631 19.a is representative of the wet period reported by Dainese (2020) with two lower
632 resistivity (150Ωm) 0.5m² regions closer to the surface below the tree ([2.0,0.0]; [3.0,-
633 0.5]) and away from the tree ([0.0,0.0]; [1.0,-0.5]) and with two higher resistivity
634 (400Ωm) 1m² regions below the tree ([2.0,-1.0]; [3.0,-2.0]) and away from the tree
635 ([0.0,-1.0]; [1.0,-2.0]). Figure 19.c represents the dry period reported by Dainese (2020),
636 with two 0.5m² regions of high resistivity (400Ωm) closer to the surface and one 1m²
637 region also with high resistivity away from the tree starting at 1m depth.

638 The measurement scheme designed was a mixture of in-hole (dipole-dipole and
639 Schlumberger, skip 0 to 6) and cross-borehole (AM-BN, AB-MN, A-BMN and A-MBN,
640 skip 0 to 6), totalling 10,298 independent data points (Sensitivity - Figure 20).

641 The inverted results (Figure 19.b-d) show that the superficial region of low (wet
642 period) and high (dry period) resistivity is well captured both in terms of geometry and
643 resistivity value, regardless of whether the resistivity value is higher or lower than the
644 background resistivity. The 1m² region of low resistivity in the wet period, and high
645 resistivity in the dry period that starts at 1m depth and is located away from the tree is
646 also well captured in terms of geometry and resistivity value. Finally, the 1m² resistivity
647 area below the tree (starting at 1m depth), that is present in the model representative of
648 the wet period (Figure 19.b), can still be easily identified, despite the fact that this is a
649 region of low sensitivity (Figure 20).

650 Therefore, this suggests that ERT could guide the installation of these local sensors.
651 if ERT surveys had been performed by Dainese (2020) prior to the installation of the
652 'Drill and Drop' sensors, the author could have potentially recognised that changes in
653 moisture content were prominent at depths below 1m; in this way the author could have
654 drilled a few deeper boreholes to capture moisture changes at deeper locations.

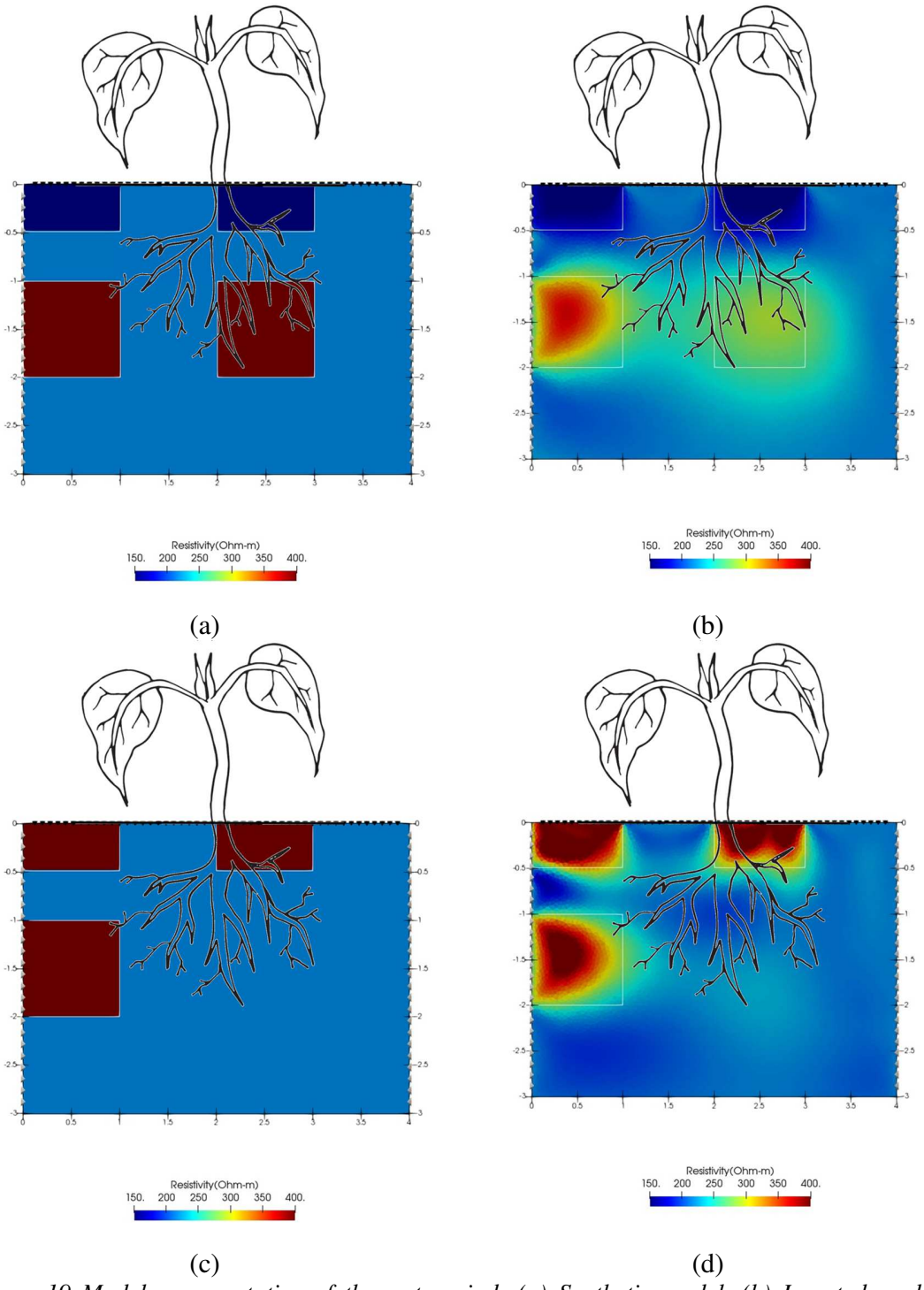

655 *Figure 19 Model representative of the wet period: (a) Synthetic model, (b) Inverted model;*

656 *Model representative of the dry period: (c) Synthetic model, (d) Inverted model*

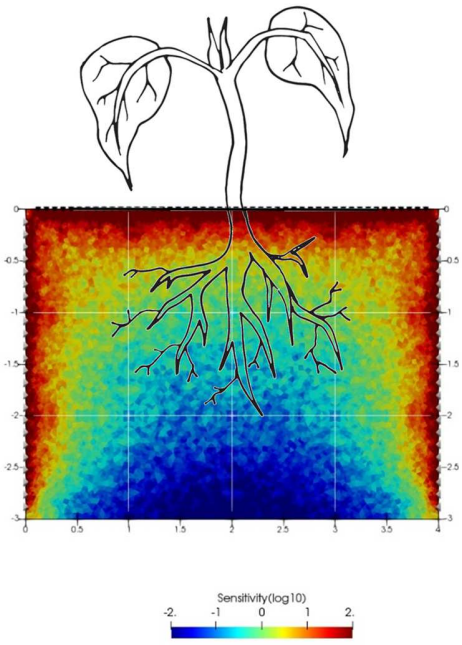

Figure 20. Measurement scheme sensitivity

5 Conclusions

The paper has presented a monitoring concept for the soil-plant continuum and focused on the measurement of water potential and flow rate of xylem water and the monitoring of soil suction and water in proximity of a tree.

Three different techniques for the measurement of xylem water tension, i.e. High-Capacity Tensiometer (HCT), Thermocouple Psychrometer (TP), and Pressure Chamber (PC), have been presented. Critical aspects of the experimental procedure including calibration, data quality check, and measurement precision have been investigated and measurement accuracy has been probed by cross-validation.

668 The HCT is the same prototype used for more than two decades in the geotechnical
669 engineering field. Details of the installation on the stem have been presented and
670 discussed to enable other researchers installing their own tensiometer. It has been shown
671 that the HCT has to be installed in pairs. In general, the measurement shows excellent
672 precision and differences between HCTs installed at close distance on the stem (<100-
673 200 mm) are generally less than 50 kPa. However, significant deviations may occur and
674 this invalidates the measurement. Deviations may occur due to ongoing cavitation or
675 healing at the measuring site.
676 The thermocouple psychrometer requires calibration by exposure of the sensor to
677 NaCl solutions of known concentration (osmotic suction). The calibration method based
678 on the use of a filter paper as proposed by the manufacturer can be potentially biased by
679 the matric suction generated by the filter paper if menisci form at the filter paper-air
680 interface. For this reason, calibration was carried out by exposing the sensor to free
681 NaCl solutions considering different air gaps between the solution and the sensor. It was
682 finally demonstrated that the procedure based on the filter paper provides reliable
683 results. It was also shown that the signal recorded by the sensor depends on both the
684 Cooling Time (the time whereby the current is circulated in the thermocouple) and the
685 Wait Time (the time at which the signal is recorded) and the same setting should be
686 therefore used for calibration and measurement.
687 As for the measurement by the Pressure Chamber, the leaf needs to be wrapped with
688 aluminium foil to establish 'hydrostatic conditions before excision according to the
689 manufacturer. It has been shown that the leaf should remain wrapped even when placing

690 it in the Pressure Chamber. The Pressure Chamber measurement appears to show
691 precision better than 100 kPa.

692 It was finally shown the measurements by these three techniques are highly
693 consistent, with the exception of the Thermocouple Psychrometer at xylem water
694 tensions below ~500 kPa.

695 The paper has therefore focused on the monitoring of soil suction using the High-
696 Capacity Tensiometer and the water content using a profile probe of second generation,
697 which is fully encapsulated and does not require the pre-installation of a casing. It was
698 shown that the major problem in water content measurement is the formation of a gap
699 between the probe and the surrounding soil. An approach has been presented to i)
700 identify the presence of the gap and ii) quantify the error associated with such a gap and
701 correct the measurement. The combined measurements of soil suction and water content
702 in the field was successfully benchmarked against water retention data acquired in the
703 laboratory in samples taken from the field.

704 Finally, it has been shown that Electrical Resistivity Tomography (ERT) can be
705 very useful to complement the local measurements of water content by the profile probe
706 by allowing capturing the spatial variability of the soil moisture distributions in
707 vegetated areas to guide the installation of these local sensors if ERT survey are carried
708 our preliminarily.

Acknowledgement

The authors wish to acknowledge the support of the European Commission via the Marie Skłodowska-Curie Innovative Training Networks (ITN-ETN) project TERRE 'Training Engineers and Researchers to Rethink geotechnical Engineering for a low carbon future' (H2020-MSCA-ITN-2015-675762)

APPENDIX 1 – EFFECT OF ROOTS ON SOIL WATER CONTENT MEASUREMENT

Soil water content θ is inferred from the measurement of the bulk soil dielectric permittivity K_a. Empirical equations are generally used to correlate K_a to θ, e.g. Topp et al. (1980) and Ledieu et al. (1986). However, the relationship between K_a and θ can also be derived theoretically using a dielectric permittivity mixing model and this allows for the quantification of the effect of roots on the water content measurement.

The simplest dielectric permittivity mixing model is the Complex Refractive Index Model (CRIM) (Leão et al. 2015). This model is first assessed for the case of a three-phase mixture (unsaturated soil in the absence of roots) and then extended to the case of a four-phase mixture (unsaturated soil with the presence of roots) to assess the error in soil water content measurement associated with the presence of roots in the measurement sampling volume.

Three-phase mixture (unsaturated soil in the absence of roots)

According to Birchak et al. (1974), the soil bulk dielectric permittivity for a three-phase mixture can be expressed as follows:

$$\sqrt{K_a} = v_a\sqrt{\varepsilon_a} + v_w\sqrt{\varepsilon_w} + v_s\sqrt{\varepsilon_s} \quad [7]$$

where v_a, v_w, and v_s are the volume fractions of the air, water, and solids respectively and ε_a, ε_w, and ε_s are the values of dielectric permittivity of the air, water, and solids respectively.

Since

$$v_w = \frac{V_w}{V} = \theta$$

$$v_s = \frac{V_s}{V} = \frac{V_s}{M_s}\frac{M_s}{V} = \frac{\rho_d}{\rho_s} \quad [8]$$

$$v_a = 1 - v_s - v_w = 1 - \frac{\rho_d}{\rho_s} - \theta$$

where V is the total volumes, V_w and V_s the volumes of water and solids respectively, M_s is the mass of solids, ρ_d and ρ_s the dry density and the density of the solids respectively. By combining Eqs. [7] and [8], a calibration curve can be derived, which has the same functional form of the equation proposed by Ledieu et al. (1986):

$$\theta = \left[\frac{1}{\sqrt{\varepsilon_w} - \sqrt{\varepsilon_a}}\right]\sqrt{K_a} - \left[\frac{\sqrt{\varepsilon_a} - \left(\sqrt{\varepsilon_a} - \sqrt{\varepsilon_s}\right)\frac{\rho_d}{\rho_s}}{\sqrt{\varepsilon_w} - \sqrt{\varepsilon_a}}\right] \quad [9]$$

This equation is compared with the very popular empirical equations presented by Topp et al. (1980) and Ledieu et al. (1986) respectively in Figure 21. It can be seen that Eq.

742 [9] is essentially equivalent to these two empirical equations and can therefore serve as a
743 basis to assess the error associated with the presence of roots.

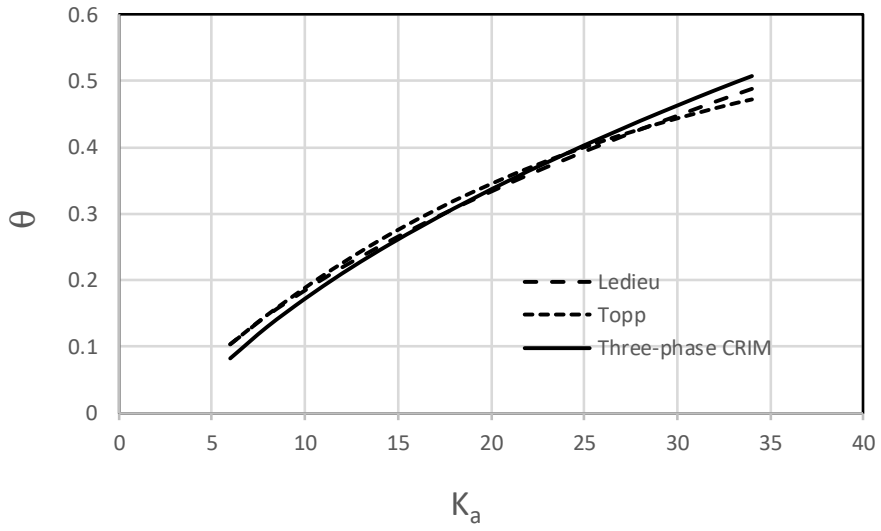

744

745 *Figure 21. Comparison of a three-phase CRIM with common empirical calibration equations*
746 *(ε_a=1, ε_s=6, ε_w=80, ρ_d=1.5 g/cm3, ρ_s=2.7 g/cm)*

747

748 *Four-phase mixture (unsaturated soil with the presence of roots)*

749 The mixing model for a four-phase mixture can be written as follows:

$$\sqrt{K_a} = v_a\sqrt{\varepsilon_a} + v_w\sqrt{\varepsilon_w} + v_s\sqrt{\varepsilon_s} + v_r\sqrt{\varepsilon_r} \quad [10]$$

750 By combining Eqs. [7] and[10], the following calibration curve is derived for the case
751 where roots are present in the measurement sampling volume

752

$$\theta = \left[\frac{1}{\sqrt{\varepsilon_w} - \sqrt{\varepsilon_a}}\right]\sqrt{K_a} - \frac{\sqrt{\varepsilon_a} - \left(\sqrt{\varepsilon_a} - \sqrt{\varepsilon_s}\right)\frac{\rho_d}{\rho_s} - \left(\sqrt{\varepsilon_a} - \sqrt{\varepsilon_r}\right)v_r}{\sqrt{\varepsilon_w} - \sqrt{\varepsilon_a}} \quad [11]$$

where ε_r and v_r are the dielectric permittivity and volume fraction of roots respectively. If the soil volumetric water content is still estimated using Eq. [7] even if roots are present in the soil (as is the case of commercial probes where the output is returned directly in terms of water content), the error can be quantifies by considering the difference between Eqs. [9] and [11] as follows:

$$\Delta\theta_{error} = \frac{\sqrt{\varepsilon_a} - \sqrt{\varepsilon_r}}{\sqrt{\varepsilon_w} - \sqrt{\varepsilon_a}}\, v_r \quad [12]$$

APPENDIX 2 – ROOT DENSITY AND ROOT VOLUME FRACTION AT RESTINCLIERES SITE

The root volume fraction was determined on core samples extracted from boreholes drilled at Restinclieres site. The total volume of the core sample was calculated from its length and the inner diameter of the casing (85 mm). The length of the core sample contained in the casing essentially coincided with the penetration in the ground indicating that negligible compression occurred during penetration. The root volume was assessed through the procedure described in detail by Dias (2019) briefly summarised here. Core samples were washed through 2mm sieve in order to collect the roots. These were placed on a scanner to acquire a high-resolution 2D image. Root dying was not required as root natural colour allowed for sufficient contrast. The software WinRhizo

(Arsenault et al. 1995) was used to analyse the images and to obtain the root cumulative volume. The roots were then removed from the scanner and placed in an oven at approximately 40°C for several days in order to obtain the dry weight and, hence, to calculate the root dry density. When the scan of all the roots contained in a core sample was considered to be excessively time consuming given the amount of roots contained, only part of the roots was scanned and the calculated volume was related to the total core sample volume proportionally to the root dry mass.

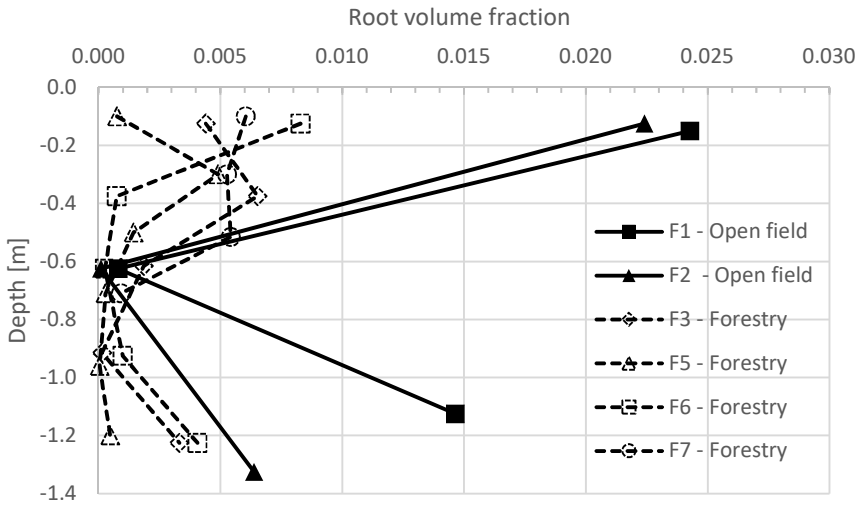

Figure 22. Profiles of root density at Restinclieres site

References

Alcántara-Ayala, I., Esteban-Chávez, O. and Parrot, J-F. (2006). Landsliding related to land-cover change: A diachronic analysis of hillslope instability distribution in the

783 Sierra Norte, Puebla, Mexico. CATENA, 65: 152-165. DOI:
784 10.1016/j.catena.2005.11.006.
785 Arsenault J.-L., S. Pouleur, C. Messier & R. Guay. 1995. WinRHIZO, a root-measuring
786 system with a unique overlap correction method. HortScience, Vol. 30, pp. 906.
787 (Abstract).
788 Balling, A. & Zimmermann, U. (1990). Comparative measurements of xylem pressure
789 of Nicotiana plants by means of the pressure bomb ad pressure probe. *Planta*,
790 182(3): 325-338
791 Birchak J R, Gardner C G, Hipp J E and Victor J M 1974 High dielectric constant
792 microwave probes for sensing soil moisture Proc. IEEE 62 93–8
793 Blanchy, G., Saneiyan S., Boyd, J., McLachlan, P., Binley, A. (2020) ResIPy, an
794 intuitive open source software for complex geoelectrical inversion/modeling.
795 Computers and Geoscience 137: 104423
796 Boyer, J. S., 1967. Leaf water potentials measured with a pressure chamber. *Plant*
797 *Physiology*, 42(1):133-7. DOI: 10.1104/pp.42.1.133.
798 Brown P., and Tanner, C. (1981). Alfalfa water potential measurement: a comparison of
799 the pressure chamber and leaf dew-point hygrometers. *Crop science*, 21(2), 240-244
800 Bulut, R. & Leong, E., (2008). Indirect measurement of suction. *Geotechnical and*
801 *Geological Engineering*, 26: 633-644. DOI: 10.1007/s10706-008-9197-0.
802 Canny, M. J. (1977). Flow and transport in plants. *Annual Review of Fluid Mechanics*, 9:
803 275–296.

804 Caruso, M, Avanzi, F. & Jommi, C. (2013). Influence of installation procedures on the
805 response of capacitance water content sensors. DOI: 10.1201/b13890-15.
806 Cassiani, G., Boaga, J., Rossi, M., Putti, M., Fadda, G., Majone, B., Bellin, A., 2016.
807 Soil-plant interaction monitoring: Small scale example of an apple orchard in
808 Trentino, North-Eastern Italy. Science of the Total Environment, 543, pp. 851-861.
809 Cassiani, G., Boaga, J., Vanella, D., Perri, M. T., Consoli, S., 2015. Monitoring and
810 modelling of soil-plant interactions: The joint use of ERT, sap flow and eddy
811 covariance data to characterize the volume of an orange tree root zone. Hydrology
812 and Earth System Sciences, 19 (5), pp. 2213-2225.
813 Consoli, S., Stagno, F., Vanella, D., Boaga, J., Cassiani, G., Roccuzzo, G., 2017. Partial
814 root-zone drying irrigation in orange orchards: Effects on water use and crop
815 production characteristics. European Journal of Agronomy, 82, pp. 190-202.
816 Corti, T., Wüest, M., Bresch, D. & Seneviratne, S. (2011). Drought-induced building
817 damages from simulations at regional scale. Natural Hazards and Earth System
818 Sciences, 11: 3335-3342. DOI: 10.5194/nhess-11-3335-2011.
819 Dainese R, Tedeschi G, Fourcaud T and Tarantino A (2020a). Measurement of xylem
820 water pressure using High-Capacity Tensiometer and benchmarking against
821 Pressure Chamber and Thermocouple Psychrometer. 4th European Conference on
822 Unsaturated Soils (E-UNSAT 2020). Lisboa, Portugal, October 19-21, 2020. DOI:
823 https://doi.org/10.1051/e3sconf/202019503014

824 Dainese, R. & Tarantino, A., 2020. Measurement of plant xylem water pressure using
825 the High-Capacity Tensiometer and implications on the modelling of soil-
826 atmosphere interaction. Geotechnique, https://doi.org/10.1680/jgeot.19.P.153
827 Dainese, R. (2020). The use of the high-capacity tensiometer as part of an integrated
828 system to monitor the soil –plant continuum for geotechnical applications. PhD
829 dissertation, University of Strathclyde, Glasgow, UK.
830 Dainese, R., Tedeschi, G., Lamarque, L., Delzon, S., Fourcaud, T., Tarantino, A.
831 (2020b). Cross-validation of High-Capacity Tensiometer and Thermocouple
832 Psychrometer for continuous monitoring of xylem water potential. Under review.
833 Deakin, N. (2005). Repair of subsidence damage: An insurer's perspective. Journal of
834 Building Appraisal. 1(3): 225-243. DOI: 10.1057/palgrave.jba.2940020.
835 Dean, T. J., Bell, J. P., & Baty, A. J. B. (1987). Soil moisture measurement by an
836 improved capacitance technique, Part I. Sensor design and performance. Journal of
837 Hydrology, 93(1-2), 67-78.
838 Dias A.S.R.A. (2019). The Effect of Vegetation on Slope Stability of Shallow
839 Pyroclastic Soil Covers. Ph.D. thesis, Naples, University of Naples Federico II,
840 University of Montpellier. https://tel.archives-ouvertes.fr/tel-02045922
841 Dixon, M. A., and Downey, A. (2015). PSY1 Stem Psychrometer Manual Ver. 4.4. ICT
842 International Pty Ltd, Armidale, Australia
843 Dixon, M. A., and M. T. Tyree (1984). A new stem hygrometer, corrected for
844 temperature-gradients and calibrated against the pressure bomb, Plant Cell Environ.,
845 7(9), 693–697.

Dolidon, N., Hofer, T., Jansky, L. and Sidle, R. (2009). Watershed and Forest Management for Landslide Risk Reduction. In Landslides - Disaster Risk Reduction, 633-649. DOI: 10.1007/978-3-540-69970-5_33.

Fan, J., Scheuermann, A., Guyot, A., Baumgartl, T., Lockington, D. A., 2015. Quantifying spatiotemporal dynamics of root-zone soil water in a mixed forest on subtropical coastal sand dune using surface ERT and spatial TDR. *Journal of Hydrology*, 523, pp. 475-488

Gladin, J., 2018. Development of miniature ERT to characterise hillslope subsurface water flow and its interplay with shallow landslides mechanisms. MSc dissertation, University of Strathclyde, Glasgow, UK.

Gonzalez-Ollauri, A. & Mickovski S.B. (2017). Hydrological effect of vegetation against rainfall-induced landslides. *Journal of Hydrology*, 549: 374-387.

Hillel, D. (1980). *Applications of soil physics*. London: Academic Press

Leão, T.P. & Perfect, E. & Tyner, John. (2015). Evaluation of Lichtenecker's mixing model for predicting effective permittivitty of soils at 50 MHZ. Transactions of the ASABE. 58. 83-91. 10.13031/trans.58.10720.

Ledieu, J., De Ridder, P., De Clerck, P., & Dautrebande, S. (1986). A method of measuring soil moisture by time-domain reflectometry. *Journal of Hydrology*, 88(3-4), 319-328.

Lev-Yadun, S. (2011). Bark. eLS.

Lu, P., Urban, L., & Zhao, P. (2004). Granier's thermal dissipation probe (TDP) method for measuring sap flow in trees: theory and practice. *Acta Botanica Sinica-English Edition*, 46(6), 631-646.

Marinho, F. A. M., Take, W. A. & Tarantino, A., 2008. Measurement of matric suction using tensiometric and axis translation techniques. *Geotechnical and Geological Engineering*, 26(6): 615-631.

Mary, B., Peruzzo, L., Boaga, J., Schmutz, M., Wu, Y., Hubbard, S. S., Cassiani, G., 2018. Small-scale characterization of vine plant root water uptake via 3-D electrical resistivity tomography and mise-à-la-masse method. Hydrology and Earth System Sciences, 22 (10), pp. 5427-5444

Meron M., Grimes D., Phene C., Davis K. 1987. Pressure chamber procedures for leaf water potential measurements of cotton. *Irrigation Sci*., 8(3): 215-222.

Mihai, A & Gerea, A & Curioni, G & Atkins, P & Hayati, F. (2019). Direct measurements of tree root relative permittivity for the aid of GPR forward models and site surveys. Near Surface Geophysics. 17. 10.1002/nsg.12043.

Pagano, L., Reder, A. & Rianna, G. (2018). The effects of vegetation on the hydrological response of silty volcanic covers. Canadian Geotechnical Journal, 56(9): 1261-1277. DOI: 10.1139/cgj-2017-0625.

Philip J. (1966). Plant Water Relations: Some Physical Aspects. Annual Review in Plant Physiology 17**,** 245-268.

PMS Instrument (2018). www.pmsinstrument.com/resources/instrument-operating-manuals

888 Pollen, N., Simon, A. & Collison, A. (2004). Advances in Assessing the Mechanical and
889 Hydrologic Effects of Riparian Vegetation on Streambank Stability. Riparian
890 Vegetation and Fluvial Geomorphology, 8: 125-139. DOI: 10.1029/008WSA10.
891 Salisbury, F.B., Ross, C.W., (1992). Plant Physiology. 4th Edition, Wadsworth
892 Publishing
893 Samouëlian, A., Cousin, I., Tabbagh, A, Bruand, A., Richard, G., 2005. Electrical
894 resistivity survey in soil science: A review. Soil and Tillage Research, 83(2), pp.
895 173-193
896 Scholander P.F., Hammel H.T. et Bradstreet E.D., 1965. Sap pressure in vascular plants.
897 Science, 148, 339-346
898 Sentek Techologies (2019). Sentek Drill & Drop Soil Moisture Probe Installation
899 Training. https://www.youtube.com/watch?v=fasI3fnNE4Y (last verified
900 28.01.2019)
901 Tarantino A., Ridley A.M. and Toll D.G. 2008. Field measurement of suction, water
902 content, and water permeability. Geotechnical and Geological Engineering, 26(6):
903 751-782.
904 Tarantino, A. & Mongiovi, L., 2002. Design and construction of a tentiometer for direct
905 measurement of matric suction. s.l., Recife, pp. 319-324.
906 Tarantino, A. & Mongiovi, L., 2003. Calibration of tensiometer for direct measurement
907 of matric suction. Geotechnique, Volume 53.
908 Tarantino, A., 2004. Panel lecture: direct measurement of soil water tension. pp. 1005-
909 1017.

910 Tedeschi G. (2019). The use of vegetation to stabilise the ground: the problem of the
911 measurement of the plant water potential. MSc dissertation, Université Grenoble
912 Alpes, Grenoble, France.
913 Toll, D.G. and Abedin, Z. and Buma, J. and Cui, Y. and Osman, A. S. and Phoon, K.K.
914 (2012). The impact of changes in the water table and soil moisture on structural
915 stability of buildings and foundation systems: systematic review CEE10-005
916 (SR90). Technical Report. Collaboration for Environmental Evidence.
917 Topp GC, Davis JL, Annan AP (1980) Electromagnetic determination of soil water
918 content: measurements in coaxial transmission lines. Water Resour Res 16:574–582
919 Turner, Neil & Spurway, RA & Schulze, E. (1984). Comparison of Water Potentials
920 Measured by In Situ Psychrometry and Pressure Chamber in Morphologically
921 Different Species. Plant physiology. 74. 316-9. 10.1104/pp.74.2.316.
922 WMO (2018). Guide to Instruments and Methods of Observation (2018 edition).
923 Volume I – Measurement of Meteorological Variables. World Meteorological
924 Organization, Geneva, Switzerland.
925
926

SUBMISSION TO
JOURNAL OF GEOMECHANICS FOR ENERGY AND THE ENVIRONMENT
SPECIAL ISSUE ON 'LOW CARBON GEOTECHNICS'

DATE:
Written: June 2020
Revised April 2021

TITLE:
Evaluation of instruments for monitoring the soil-plant continuum

AUTHORS:
Roberta Dainese[1,2,3]
Bruna de Carvalho Faria Lima Lopes[1]
Thierry Fourcaud[2]
Alessandro Tarantino[1]

AFFILIATION:
[1] Department of Civil and Environmental Engineering, University of Strathclyde, Glasgow, UK
[2] CIRAD, UMR AMAP, F-34398 Montpellier, France
[3] AMAP, Univ Montpellier, CIRAD, CNRS, INRAE, IRD, Montpellier, France

CORRESPONDING AUTHOR:
Dr Roberta Dainese
Department of Civil and Environmental Engineering
University of Strathclyde
James Weir Building - Level 5
75 Montrose Street - Glasgow G1 1XJ, Scotland, UK
E-mail: roberta.dainese.rd@gmail.com

KEYWORDS
High-Capacity Tensiometer, Pressure Chamber, Thermocouple Psychrometer, Xylem water tension, Soil water tension, Time Domain Reflectometry, Electrical Resistivity Tomography